Utilizing the polar cap index to explore strong driving of polar cap dynamics

Ye Gao,[1,2] Margaret G. Kivelson,[1,2,3] Aaron J. Ridley,[3] James M. Weygand,[2] and Raymond J. Walker[1,2]

Received 19 August 2011; revised 14 April 2012; accepted 3 June 2012; published 18 July 2012.

[1] The polar cap, defined as a region of open magnetic flux, is an ideal region in which to investigate how properties of the solar wind directly affect the magnetosphere. For such studies, the polar cap (PC) index provides a useful characterization of the state of the polar ionosphere. In this paper, we study how polar cap properties, quantified by the PC index, depend on solar wind parameters and other geomagnetic indices during intervals of exceptionally large (10 mV/m) merging electric field. Using 53 one to two-day intervals that include such extreme fields, we find that the PC index correlates strongly with the modified electric field ($E_{K\text{-}R}$) proposed by Kivelson and Ridley (2008). Here, $E_{K\text{-}R}$ is a form representative of several models in which the electric field imposed on the ionosphere by magnetopause reconnection saturates for extreme solar wind driving. However, there are anomalous events during which the auroral oval expanded poleward to the latitude of the PC index station and the index increased because of proximity to auroral zone currents. It is found that nightside magnetospheric processes, as represented by AL, make a significant contribution to the PC index. A linear regression analysis shows that the portion of the PC index directly driven by the solar wind electric field outweighs the contribution arising from energy release in the magnetotail by roughly a factor of 2. Neither the solar wind dynamic pressure (P_{dyn}) nor jumps in P_{dyn} are found to directly contribute to the PC index. However, there exists some correlation between the PC index and P_{dyn}, because of the common dependence of $E_{K\text{-}R}$ and P_{dyn} on the solar wind number density.

Citation: Gao, Y., M. G. Kivelson, A. J. Ridley, J. M. Weygand, and R. J. Walker (2012), Utilizing the polar cap index to explore strong driving of polar cap dynamics, *J. Geophys. Res.*, *117*, A07213, doi:10.1029/2011JA017087.

1. Introduction

[2] The magnetosphere-ionosphere dynamo is primarily governed by two types of processes. They have been categorized as directly driven processes and unloading processes [*McPherron and Baker*, 1993]. A directly driven process is one in which the output, which is often measured by geomagnetic indices, is proportional to the solar wind input with at most a small time delay. The two-cell current system, or "disturbance polar of the second type" (DP2) [*Iijima and Nagata*, 1972; *Kokubun*, 1972], is powered by the direct projection of the solar wind electric field onto the conducting ionosphere. In contrast, an unloading process is one in which the magnetosphere accumulates energy without a corresponding output until, after a substantial time delay, energy is unloaded, often abruptly. As envisioned by *Akasofu* [1979a], the unloading process is internal to the magnetosphere and hence its wave form bears little resemblance to the input. The one-cell intensification, or DP1, of the westward electrojet near midnight is powered by processes internal to the plasma sheet [*McPherron and Baker*, 1993]. Measured by the AL index, it has been shown that magnetospheric activity is controlled by both driven processes and unloading processes [e.g., *Bargatze et al.*, 1985]. The polar cap is typically open to the solar wind, so it is believed to respond primarily to the solar wind direct driving [e.g., *Troshichev et al.*, 1988, 1996]. In previous studies [e.g., *Troshichev et al.*, 1988], direct coupling between the solar wind and the polar cap was established by correlating a polar cap magnetic index and the solar wind electric field [*Kan and Lee*, 1979].

[3] The polar cap (PC) index used in the analysis was introduced by *Troshichev et al.* [1988] as an instantaneous indicator of geomagnetic activity over the polar cap caused by the interplanetary magnetic field (IMF) and the solar wind. The PC index, therefore, has been interpreted as a way of quantifying the portion of magnetospheric activity directly driven by the solar wind [*Bargatze et al.*, 1985]. The algorithm from which the index is calculated is based on a

[1]Department of Earth and Space Sciences, UCLA, Los Angeles, California, USA.
[2]Institute of Geophysics and Planetary Physics, UCLA, Los Angeles, California, USA.
[3]Department of Atmospheric, Oceanic and Space Sciences, University of Michigan, Ann Arbor, Michigan, USA.

Corresponding author: Y. Gao, Department of Earth and Space Sciences, UCLA, 595 Charles Young Dr. East, Los Angeles, CA 90095-1567, USA. (ygao@igpp.ucla.edu)

0148-0227/12/2011JA017087

statistical analysis of the relationship between variations in merging electric field ($E_{\text{K-L}}$) [*Kan and Lee*, 1979] and geomagnetic perturbations of the local magnetic field (ΔF_{PROJ}) at a high latitude station on the Earth's surface. The merging electric field is related to the solar wind magnetic field, $\boldsymbol{B}$, and velocity, $\boldsymbol{u}$, by

$$E_{\text{K-L}} = uB_{YZ}\sin^2\theta/2, \tag{1}$$

where u is the magnitude of the solar wind velocity, $B_{YZ} = (B_Y^2 + B_Z^2)^{1/2}$ in the GSM coordinate system, and θ is the IMF clock angle measured from the GSM Z axis. The surface magnetic field perturbation is projected to the "optimum direction" perpendicular to the mean transpolar DP2 equivalent current to get ΔF_{PROJ}, which can also be expressed as

$$\Delta F_{\text{PROJ}} = \Delta H\sin\gamma + \Delta D\cos\gamma, \tag{2}$$

where

$$\gamma = \lambda \pm D_{\text{E}} + \varphi + \text{UT}\cdot 15^\circ, \tag{3}$$

ΔH and ΔD are deviations in the ground horizontal (H and D) magnetic field components from a pre-established quiet level. Two near-pole magnetic observatories have been used to derive the PC index: Qaanaaq in Greenland at 86.5° magnetic latitude for northern PC index (PCN), and Vostok in Antarctica at −83.4° magnetic latitude for southern PC index (PCS) [*Troshichev et al.*, 2006]. For PCN, the reference is the internal field level, whereas, for PCS, the reference is the quiet level, which is the sum of the internal field and the QDC (quiet day curve) [*Janzhura and Troshichev*, 2008]. In equation (3), D_{E} is the station's declination angle with "+" for the southern hemisphere and "−" for the northern hemisphere, λ is its geographical longitude, and φ, the optimum direction angle, is the UT-dependent angle between the average DP2 transpolar current and the noon-midnight meridian [*Stauning*, 2011]. *Troshichev et al.* [1988] showed that ΔF_{PROJ} varies approximately linearly with the merging electric field, i.e.,

$$\Delta F_{\text{PROJ}} \approx \alpha E_{\text{K-L}} + \beta, \tag{4}$$

where α and β are constants estimated from regression between ΔF_{PROJ} and $E_{\text{K-L}}$. The PC index is defined as

$$\text{PC} = (\Delta F_{\text{PROJ}} - \beta)/\alpha\eta, \tag{5}$$

where $\eta = 1$ mV/m is a normalization coefficient introduced to make the PC index dimensionless. Thus, by its definition, the PC index directly approximates the merging electric field, i.e.

$$\text{PC} \approx E_{\text{K-L}}. \tag{6}$$

Stauning [2011] discussed the derivation of the PC index in more detail.

[4] Since its definition, various statistical analyses have demonstrated that the PC index can be regarded as an instantaneous estimator of diverse ionospheric phenomena. For example, *Troshichev et al.* [1996] related the PC index to the cross polar cap potential (Φ_{PC}) measured by EXOS-D and obtained a linear relationship,

$$\Phi_{\text{PC}}[\text{kV}] \approx 19.35\text{PC} + 8.78. \tag{7}$$

Ridley and Kihn [2004] took seasonal effects into account and proposed a different formula to convert from polar cap index to the cross polar cap potential measured by AMIE,

$$\Phi_{\text{PC}}[\text{kV}] \approx 29.28 - 3.31\sin(T + 1.49) + 17.81\text{PC}, \tag{8}$$

where T is the month of the year normalized to 2π (e.g., January = 0, July = $6 \times 2\pi/12 = \pi$, December = $11 \times 2\pi/12$). *Troshichev et al.* [2000] related the cross polar cap electric field measured by DMSP to the PC index using a second order polynomial. *Fiori et al.* [2009] confirmed the relationship proposed by *Troshichev et al.* [2000] by obtaining a similar result between the ionospheric plasma convection velocity and the PC index. *Liou et al.* [2003] examined the statistical relationship between auroral power and the polar cap index and found a reasonably large correlation coefficient ($\rho \approx 0.7$). *Chun et al.* [1999, 2002] have shown that the PC index can serve as a proxy for the hemispheric Joule heating production rate and claimed that it is possible to predict the Joule heating pattern from the PC index. Since the algorithm used to derive the PC index has evolved dramatically [*Vennerstrøm*, 1991; *Troshichev et al.*, 2006; *Stauning*, 2011], discrepancies in results from different studies may be attributed in part to the use of different forms of the PC index.

[5] Despite the general success in describing how the solar wind affects the polar ionosphere using the PC index, few studies have paid attention to times of intense geomagnetic activity. However, the saturation of the cross polar cap potential at such times has been extensively discussed [e.g., *Russell et al.*, 2000; *Nagatsuma*, 2002; *Shepherd et al.*, 2002; *Siscoe et al.*, 2002; 2004; *Kivelson and Ridley*, 2008]. In exploring the physical mechanism of the cross polar cap potential saturation, *Kivelson and Ridley* [2008] took into consideration the partial reflection of the merging electric field at the top of the ionosphere and proposed that the electric field observed in the ionosphere would differ from that directly imposed from the solar wind. The modified field will be designated as the Kivelson-Ridley electric field ($E_{\text{K-R}}$), defined as

$$E_{\text{K-R}} = E_{\text{K-L}}2\Sigma_{\text{A}}/(\Sigma_{\text{A}} + \Sigma_{\text{P}}), \tag{9}$$

where $2\Sigma_{\text{A}}/(\Sigma_{\text{P}} + \Sigma_{\text{A}})$ is the transmission coefficient. In equation (9), Σ_{P} is the ionospheric Pedersen conductance, and Σ_{A} is the Alfvén conductance of the Alfvén wing. Here,

$$\Sigma_{\text{A}} = 1/\mu_0 v_{\text{A}}, \tag{10}$$

where v_{A} is the Alfvén velocity in the solar wind, which is related to the solar wind parameters through

$$v_{\text{A}} = B/(\mu_0\rho_{\text{sw}})^{1/2}. \tag{11}$$

In equation (11), B is the IMF magnitude, ρ_{sw} is the solar wind mass density, and $\mu_0 = 4\pi \times 10^{-7}$ H/m is the permeability of free space. Under typical solar wind conditions, e.g., $E_{\text{K-L}} < 5$ mV/m, Σ_{A} is slightly larger than but close to Σ_{P}. Thus, $E_{\text{K-R}} \approx 1.2E_{\text{K-L}}$. Nevertheless, under intense solar wind driving, e.g., $E_{\text{K-L}} > 10$ mV/m, Σ_{A} decreases significantly, i.e., $\Sigma_{\text{A}} < \Sigma_{\text{P}}$, and thus, $E_{\text{K-R}} < E_{\text{K-L}}$. It has been argued that $E_{\text{K-R}}$ serves as a better indicator of the electric field in the ionosphere caused by the dayside reconnection

than does $E_{K\text{-}L}$, especially when $E_{K\text{-}L}$ is unusually large [*Kivelson and Ridley*, 2008; *Borovsky et al.*, 2009]. Consequently, it is of interest to consider which of the two forms of the electric field correlates more closely with that driving convection in the polar cap by investigating the behavior of the PC index during exceptionally active intervals.

[6] Different mechanisms have been proposed to explain the saturation of cross polar cap potential under strong solar wind driving. For example, *Siscoe et al.* [2002, 2004], who adopted and developed the model of *Hill et al.* [1976], argued that the saturation of cross polar cap potential results from a feedback in which the magnetic field generated by the Region-1 current becomes comparable to and opposes the Earth's dipole field at the magnetopause where reconnection occurs. By significantly weakening the field that is reconnecting, the Region-1 current ultimately limits how fast reconnection occurs, resulting in the saturation of cross polar cap potential. Although the physical mechanism proposed by *Siscoe et al.* [2002, 2004] is fundamentally different from that by *Kivelson and Ridley* [2008], the predicted electric fields from the two models are similar. It is not the purpose of this paper to explore which model is correct, and essentially, all saturation models predict the saturated electric field in forms similar to equation (9) [e.g., *Borovsky et al.*, 2009]. Thus, we employ $E_{K\text{-}R}$ as representative of the electric field imposed on the polar ionosphere by magnetopause reconnection that takes saturation into account. For other models of cross polar cap potential saturation, see *Borovsky et al.* [2009].

[7] Unlike the PC index, the auroral electrojet indices AL, AE are meant to estimate the release of energy stored in the magnetotail during substorms. Although it is often assumed that the PC index is not significantly affected by nightside substorm dynamics, previous studies have shown that the correlation between the PC and the AE indices is high. *Vennerstrøm et al.* [1991] showed that the PC index correlates better with the AE and AL indices, than with the AU index, the linear correlation coefficient being equal to 0.8–0.9 in winter and 0.6–0.8 in summer. *Huang* [2005] examined the relationship between the PC index and substorm activity and found that the PC index is enhanced after substorm onset. Thus, the PC index, due to its great simplicity, provides an excellent tool for quantifying the influence on the polar cap dynamics of both the solar wind driver and the magnetospheric unloading process.

[8] The solar wind dynamic pressure (P_{dyn}) has also been found to influence the PC index [e.g., *Lukianova*, 2003]. *Lukianova* [2003] examined the relationship between $E_{K\text{-}L}$, P_{dyn}, and the PC and AE indices in detail and concluded that the PC index directly responds to an enhancement in P_{dyn} and the influence of P_{dyn} pulses can be as large as the influence of southward IMF. *Troshichev et al.* [2007] carried out a superposed epoch analysis of 62 pressure jumps between 1998 and 2002 and concluded that the solar wind pressure growth rate (i.e., the jump in power, dP_{dyn}/dt) appears to be the second most important factor after $E_{K\text{-}L}$ for controlling variations of the PC index [see also *Stauning and Troshichev*, 2008]. *Stauning et al.* [2008] examined the relationship between the PC index and the dynamic pressure for typical conditions and found little correlation between the PC index and the steady state solar wind dynamic pressure. *Huang* [2005] performed both case study and statistical analysis on the role of solar wind dynamic pressure pulse on the PC index under many solar wind conditions and concluded that, on average, the solar wind dynamic pressure is less important than both the solar wind electric field and substorm activity.

[9] In this study, we investigate the influence of the solar wind and geomagnetic activity on the polar cap dynamics by studying the relationship between the PC index and various solar wind parameters as well as geomagnetic indices, focusing on intervals of high activity. In section 2, we describe the data used. In section 3, we apply regression analysis to 53 one to two-day intervals from 1998 to 2006 with subintervals during which $E_{K\text{-}L}$ exceeds 10 mV/m. We find that (1) the PC index correlates better with $E_{K\text{-}R}$ than with $E_{K\text{-}L}$ especially when $E_{K\text{-}R}$ differs significantly from $E_{K\text{-}L}$; (2) the PC index is influenced by both external and internal flows, i.e., by the solar wind as characterized by $E_{K\text{-}L}$ or $E_{K\text{-}R}$ and by magnetotail activity as represented by the AL index; (3) the dayside input, or equivalently, the electric field of the solar wind contributes more than the nightside input or, equivalently, the energy release in substorms; (4) if the effect of varying solar wind density is attributed to the modified electric field, $E_{K\text{-}R}$, the residual PC index does not respond directly to P_{dyn} or jumps in P_{dyn}; (5) the auroral oval may, on occasion, expand poleward to as far north as Qaanaaq (86.5° magnetic latitude), in which case the PC index records the effects of currents flowing on nearby closed field lines and may become unusually large. Finally, in section 4, we summarize the results and discuss the relationship between polar cap responses as characterized by the PC index and solar wind parameters and auroral electrojet activity.

2. Data

[10] In this study, we use 1-min values of the northern PC index (PCN) where coverage is more complete than PCS. We use PCS only as a diagnostic tool. For each event identified, we have compared the PCN and PCS to verify the quality of the PCN index except those from 2003 during which the PCS data are unavailable. Despite some differences in values, the indices generally change in correspondence with each other. The data used in this paper were acquired between 1998 and 2006, and the correlations reported are those for indices obtained as follows: the PCN index comes from magnetic data of the Qaanaaq station (86.5° magnetic latitude) and is produced by the Danish National Space Institute (DTU space); the PCS index is from Vostok (−83.4° magnetic latitude) magnetic data and is produced by the Arctic and Antarctic Research Institute [*Troshichev and Lukianova*, 2002].

[11] Data on the solar wind are provided by instruments on the ACE (Advanced Composition Explorer) spacecraft. ACE was launched on 25 August 1997 to the Lagrange Point 1 ($L1$) to serve as an instantaneous monitor of the solar wind conditions. We use 1-min magnetic field vectors and plasma moments obtained from 1998 to 2006 provided by the Magnetic Field (MAG) and Solar Wind Electron, Proton, and Alpha Monitor (SWEPAM) instrument. The GSM coordinate system is adopted for analyzing plasma velocity and magnetic field data. The solar wind observations have

Table 1. One to Two-Day Intervals With Subintervals During Which $E_{K\text{-}L} > 10$ mV/m Between 1998 and 2006 Used in This Study

Number	Time	Number	Time	Number	Time
1.	4 May 1998	19.	27 March 2001	37.	14 October 2003
2.	29 May 1998	20.	31 March 2001	38.	24 October 2003
3.	26–27August 1998	21.	4 April 2001	39.	31 October 2003
4.	24–25 September 1998	22.	8 April 2001	40.	4 November 2003
5.	8 November 1998	23.	11–12 April 2001	41.	20 November 2003
6.	18 February 1999	24.	18 April 2001	42.	6 January 2004
7.	22 September 1999	25.	28 April 2001	43.	22 January 2004
8.	21–22 October 1999	26.	17 August 2001	44.	25–26 July 2004
9.	27 January 2000	27.	3 October 2001	45.	7–8 November 2004
10.	12 February 2000	28.	21 October 2001	46.	7 January 2005
11.	6 April 2000	29.	30 December 2001	47.	17 January 2005
12.	23–24 May 2000	30.	17 April 2002	48.	21 January 2005
13.	8 June 2000	31.	19–20 April 2002	49.	8 May 2005
14.	13 July 2000	32.	23 May 2002	50.	15 May 2005
15.	16 July 2000	33.	7 September 2002	51.	24 August 2005
16.	12 August 2000	34.	21 November 2002	52.	15 September 2005
17.	17–18 September 2000	35.	29–30 May 2003	53.	14–15 December 2006
18.	5 October 2000	36.	18 August 2003		

been propagated to $X_{GSM} = 17R_E$ using the technique of *Weimer et al.* [2003] and *Weimer* [2004].

[12] The AE index from the World Data Center is derived from geomagnetic variations in the horizontal component observed at 12 selected observatories along the auroral zone in the northern hemisphere. AU and AL form the upper and lower envelopes of the superposed plots of all the data from these stations as functions of UT. The difference, AU minus AL, defines the AE index, and the mean value of the AU and AL, i.e., (AU + AL)/2, defines the AO index.

3. Analysis

[13] Since the PC index is measured at a single station, non-negligible statistical fluctuations are inevitable. Thus, in this study, we concentrate on geomagnetically active times when the PC index exceeds a baseline value. We limit our study to extreme cases that include intervals during which $E_{K\text{-}L}$ exceeds 10 mV/m and typically PC > 5. This criterion leaves us 53 one to two-day intervals between 1998 and 2006 (shown in Table 1).

3.1. The Kivelson-Ridley Electric Field, $E_{K\text{-}R}$

[14] In this study, $E_{K\text{-}R}$ is used as representative of the polar cap electric field imposed by dayside reconnection that is modified to account for saturation. According to *Kivelson and Ridley* [2008], when the impedance of the solar wind across open polar cap field lines dominates the impedance of the ionosphere, Alfvén waves incident from the solar wind are partially reflected, reducing the strength of the signal in the polar cap. Thus the ratio of the cross polar cap electric field to the reconnection electric field imposed by the solar wind is $2\Sigma_A/(\Sigma_A + \Sigma_P)$. This form has the interesting property of depending on both solar wind and ionospheric properties. Here, $\Sigma_A = 1/\mu_0 v_A$ is the Alfvén conductance of the solar wind. In addition, if the density variation from solar wind to ionosphere along a field line is taken into account, a corrected form would replace $\Sigma_A = 1/\mu_0 v_A$ by

$$\Sigma_A = \left(\rho_{pc}/\rho_{sw}\right)^{1/4}(1/\mu_0 v_A), \qquad (12)$$

where ρ_{pc}, which depends on ρ_{sw}, is the mass density in the low altitude polar cap (e.g., $2R_E$) at the top of the ionosphere. Probable values of $(\rho_{pc}/\rho_{sw})^{1/4}$, insensitive to solar wind conditions, are likely to differ from 1 by no more than a factor of 2. As the values of ρ_{pc} are not routinely measured [*Kitamura et al.*, 2011], one should use $\Sigma_A = 1/\mu_0 v_A$ with the understanding that this introduces errors of a few tens of percent in our calculations (for details, please refer to the appendix of *Kivelson and Ridley* [2008]). Σ_P is the ionospheric Pedersen conductance chosen to be 10S [*Kivelson and Ridley*, 2008]. We have also run our analyses using values of 5S and 15S for Σ_P and found that our conclusion remains unchanged from those reached when Σ_P is 10S.

[15] We first compare the correlation between the PC index and $E_{K\text{-}R}$ with correlations between the PC index and the following previously proposed coupling functions between the solar wind and the Earth's magnetosphere [*Troshichev et al.*, 1996]:

[16] 1. energy coupling function of *Akasofu* [1979b], $\varepsilon = uB_{YZ}^2 \sin^4\theta/2$;

[17] 2. tangential interplanetary electric field, $E_T = uB_{YZ}$;

[18] 3. merging electric field [*Kan and Lee*, 1979], $E_{K\text{-}L} = uB_{YZ}\sin^2\theta/2$;

[19] 4. polar cap voltage of *Reiff and Luhmann* [1986], $\Phi_{PC,R\text{-}L} \propto uB_{YZ}\sin^4\theta/2$;

[20] 5. polar cap voltage of *Pudovkin et al.* [1982], $\Phi_{PC,P} \propto n^{-1/2}B_{YZ}^2\sin^3\theta/2$.

[21] Table 2 shows the correlation coefficients among the PCN index and those coupling functions as well as the solar

Table 2. Correlation Coefficients Linking PCN With Various Coupling Functions Purported to Quantify the Strength of the Direct Interaction With the Solar Wind[a]

	PCN	ε	P_{dyn}	E_T	$E_{K\text{-}L}$	$E_{K\text{-}R}$	$\Phi_{PC,R\text{-}L}$	$\Phi_{PC,P}$
PCN	1.00	0.62	0.69	0.69	0.71	**0.87**	0.71	0.46
ε		1.00	0.22	0.98	0.98	0.75	0.98	0.95
P_{dyn}			1.00	0.43	0.36	0.70	0.34	0.01
E_T				1.00	0.96	0.83	0.94	0.84
$E_{K\text{-}L}$					1.00	0.86	0.99	0.90
$E_{K\text{-}R}$						1.00	0.86	0.57
$\Phi_{PC,R\text{-}L}$							1.00	0.90
$\Phi_{PC,P}$								1.00

[a]Symbols are defined in the text. The solar wind are propagated to $X_{GSM} = 17R_E$ using the technique of *Weimer et al.* [2003] and *Weimer* [2004] without additional time shift.

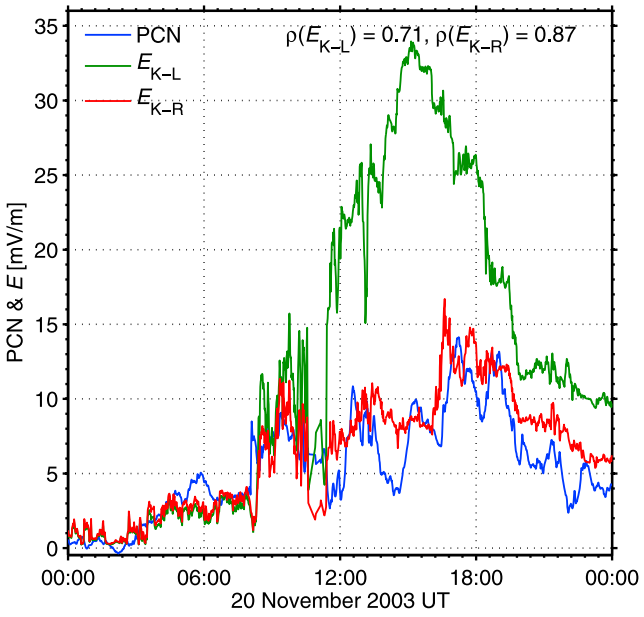

Figure 1. The PCN index, merging electric field ($E_{K\text{-}L}$) and Kivelson-Ridley electric field ($E_{K\text{-}R}$) on 20 November 2003. Here, $E_{K\text{-}L}$ and $E_{K\text{-}R}$ are calculated from the propagated solar wind data without additional time shift. The blue line is the measured PCN index. The green line is the merging electric field in mV/m. The red line is the Kivelson-Ridley electric field in mV/m evaluated for Σ_P = 10S.

wind dynamic pressure during an event on 20 November 2003. The PCN index correlates best with $E_{K\text{-}R}$, with correlation coefficient 0.87. In Figure 1, the time series of the PCN index (blue), the merging electric field (green) and the Kivelson-Ridley electric field (red) are plotted. For values of $E_{K\text{-}L} < 5$ mV/m, there is little difference between $E_{K\text{-}L}$ and $E_{K\text{-}R}$, but for larger values of $E_{K\text{-}L}$ and especially between 1200UT and 1800UT, $E_{K\text{-}L}$ and $E_{K\text{-}R}$ differ considerably. The PCN index obviously follows $E_{K\text{-}R}$ more closely.

[22] We also compare correlations obtained from regression analyses with PCN as the dependent variable and both $E_{K\text{-}R}$ and $E_{K\text{-}L}$ as independent variables, i.e.,

$$\mathrm{PCN}_{\mathrm{regress}} = \beta_0{}^{(1)} + \beta_1{}^{(1)} E_{K\text{-}L}, \tag{13}$$

and

$$\mathrm{PCN}_{\mathrm{regress}} = \beta_0{}^{(2)} + \beta_1{}^{(2)} E_{K\text{-}R}, \tag{14}$$

where $\beta_0^{(1)}$, $\beta_1^{(1)}$, $\beta_0^{(2)}$, and $\beta_1^{(2)}$ are regression coefficients. Recall that we used the *Weimer et al.* [2003] and *Weimer* [2004] technique to propagate the solar wind from ACE to $X_{GSM} = 17R_E$. *Ashour-Abdalla et al.* [2008] compared properties of the solar wind propagated from $L1$ with properties directly observed by a near Earth satellite (e.g., Geotail). They found general consistency between the propagated solar wind and observed solar wind, although they differed in some cases. Differences are more frequently observed during active times [see also *Ridley*, 2000]. Therefore, we have added time shifts for each individual event to obtain the maximum cross-correlations between PCN and $E_{K\text{-}L}$ and between PCN and $E_{K\text{-}R}$ respectively. The added time shifts are typically between 0 and 20 min with peak occurrence close to 12 min. Given the great complexity of establishing time delays between solar wind quantities and PCN, a cross-correlation analysis provides only an approximation to the precise time delay, but the uncertainty does not mask the correlations that we are studying.

[23] In order to compare the degree to which the PCN index can be predicted from $E_{K\text{-}L}$ and $E_{K\text{-}R}$ through linear regression, two statistics are calculated: R^2 and error variance. R^2, often referred to as the coefficient of determination or prediction efficiency, is defined as

$$R^2 = 1 - SS_{\mathrm{Res}}/SS_{\mathrm{Total}}. \tag{15}$$

Here, the residual sum of squares, SS_{Res}, is defined in terms of the deviations of measurements from a linear regression model as

$$SS_{\mathrm{Res}} = ||\boldsymbol{y} - \hat{\boldsymbol{y}}||^2, \tag{16}$$

where $\boldsymbol{y}$ is the vector of observations, $\hat{\boldsymbol{y}}$ is the vector of least square fits, and $\|\boldsymbol{x}\|$ represents the Euclidean norm of a vector $\boldsymbol{x}$. Similarly, the total sum of squares, SS_{Total}, is defined as

$$SS_{\mathrm{Total}} = ||\boldsymbol{y} - \bar{y}\mathbf{1}||^2, \tag{17}$$

where $\bar{y}$ is the sample mean, and $\mathbf{1}$ is given by $\mathbf{1} = (1, \ldots, 1)^{\mathrm{T}}$. R^2, which takes values between 0 and 1, i.e., $R^2 \in [0, 1]$, represents the proportion of variation in the dependent variable that is explained by the model [*Myers*, 2000]. For example, a value such as $R^2 = 0.7$ can be interpreted as meaning: "Approximately 70% of the variation in the dependent variable can be explained by the assumed independent variables. The remaining 30% must be explained by unknown variables or inherent variability." In a linear regression analysis, which is the model that we are employing here, R^2 is the square of the correlation coefficient (ρ). Although statistically only R^2 of the variation can be attributed to the independent variables tested, in this study, $R^2 \geq 0.5$ is taken to indicate adequacy of fit. The criterion is a weak one, but the majority of our cases (33 of 53) satisfy the stronger criterion $R^2 \geq 0.6$ and 21 of our 53 cases satisfy the criterion $R^2 \geq 0.7$.

[24] The error variance is estimated from the variance of the residuals [*Myers*, 2000], i.e.,

$$\sigma^2 = SS_{\mathrm{Res}}/(n - p), \tag{18}$$

where n is the number of observations, and p is the number of parameters. For example, for equation (33) later used in this paper, $p = 3$. For the event of 20 November 2003, the results are shown in Figure 2.

[25] Because the magnitudes of the independent variables can be quite different, it is helpful to normalize them so they all have similar ranges. The weighting of the normalized independent variable can then represent its importance. The normalization is achieved through replacement of the variable X with mean μ_X and standard deviation σ_X by its z-score, which is specified as

$$zs(X) = (X - \mu_X)/\sigma_X. \tag{19}$$

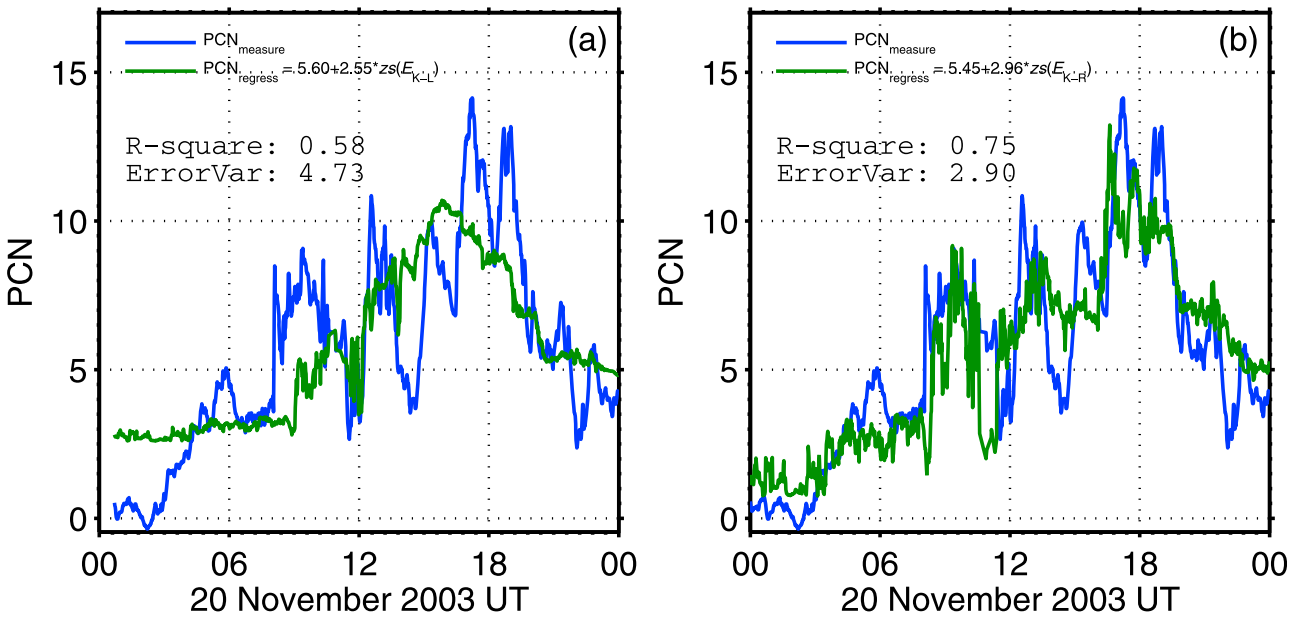

Figure 2. Comparison between the measured PCN index and the predicted PCN index based on solar wind parameters for the storm of 20 November 2003. The blue line is the measured PCN index. The green line is the predicted PCN index based on a linear regression from (a) the solar wind merging electric field ($E_{K\text{-}L}$) and (b) the Kivelson-Ridley electric field ($E_{K\text{-}R}$). Additional time shifts have been added to the propagated solar wind data to achieve the highest correlation between PCN and $E_{K\text{-}L}$ and between PCN and $E_{K\text{-}R}$ respectively. R^2 and error variance are calculated to estimate the goodness of fit.

The normalized quantity has expectation 0 and standard deviation 1. For example, in Figure 2a, the relation between the PCN index and $zs(E_{K\text{-}L})$ is summarized as

$$\mathrm{PCN}_{\mathrm{regress}} = 5.60 + 2.55 zs(E_{K\text{-}L}). \quad (20)$$

For a normalized independent variable, the regression coefficient indicates the weight of this factor. Thus, if multiple independent variables contribute to the PCN index, a direct comparison of regression coefficients linking PCN and the corresponding z-score representations reveals the relative importance among all the independent variables. In Figure 2b, such a relation between the PCN index and $E_{K\text{-}R}$ yields

$$\mathrm{PCN}_{\mathrm{regress}} = 5.45 + 2.96 zs(E_{K\text{-}R}). \quad (21)$$

R^2 and error variance have been calculated for both $E_{K\text{-}L}$ and $E_{K\text{-}R}$. The PCN inferred from $E_{K\text{-}R}$ corresponds more closely to the measured PCN (Figure 2b) than does the PCN predicted from $E_{K\text{-}L}$ (Figure 2a). A direct comparison of the regression coefficient between PCN and $E_{K\text{-}R}$ (2.96) with that between PCN and $E_{K\text{-}L}$ (2.55) supports the stronger predictability of PCN from $E_{K\text{-}R}$, which is further confirmed by R^2 and error variance. The R^2 is significantly higher for $E_{K\text{-}R}$ (0.75) than for $E_{K\text{-}L}$ (0.58), while the error variance for $E_{K\text{-}R}$ (2.90) is significantly lower than for $E_{K\text{-}L}$ (4.73).

[26] Figure 3 shows another event on 8 November 1998, and again the estimates of the quality of the prediction favor $E_{K\text{-}R}$. When $E_{K\text{-}L}$ is significantly different from $E_{K\text{-}R}$, the PCN indices predicted from $E_{K\text{-}L}$ and $E_{K\text{-}R}$ differ considerably. However, most of the time, the difference between $E_{K\text{-}L}$ and $E_{K\text{-}R}$ is not significant, because for typical solar wind properties, the factor multiplying $E_{K\text{-}L}$ in equation (9) is close to 1. Consequently, most of the time, there is an insignificant improvement in changing the basis of prediction from $E_{K\text{-}L}$ to $E_{K\text{-}R}$.

[27] For clarity, we explicitly define ΔR^2 as

$$\Delta R^2 = R^2 \text{ of equation (14)} - R^2 \text{ of equation (13)}. \quad (22)$$

Figure 4 displays ΔR^2 for 53 cases in ΔR^2 ascending order. Positive values of ΔR^2 indicate improvement by switching from $E_{K\text{-}L}$ to $E_{K\text{-}R}$ as independent variable, while negative values mean poorer predictions. R^2 increases by using $E_{K\text{-}R}$ as an independent variable with a few exceptions. Furthermore, the typical negative values are small compared with most of the positive values.

3.2. The Influence of Pedersen Conductance, Σ_P

[28] In equation (9), Σ_P is an important parameter in determining $E_{K\text{-}R}$, but it cannot be precisely estimated. Thus, it is necessary to test the sensitivity of our results to the assumed value of Σ_P (10S). If Σ_P is allowed to take values continuously from 0 to ∞, then $E_{K\text{-}R}$ becomes a function of Σ_P, i.e.,

$$E_{K\text{-}R} = E_{K\text{-}R}(\Sigma_P), \text{where } \Sigma_P \in [0, \infty). \quad (23)$$

We first notice that the similarity between $E_{K\text{-}L}$ and $E_{K\text{-}R}$, as measured by their correlation coefficient (ρ), i.e.,

$$\rho(\Sigma_P) = \rho(E_{K\text{-}L}, E_{K\text{-}R}(\Sigma_P)), \quad (24)$$

decreases as Σ_P increases. This can be partly verified by examining the values of ρ at $\Sigma_P = 0$ and when Σ_P approaches ∞. At $\Sigma_P = 0$, since $E_{K\text{-}R}(0) = 2E_{K\text{-}L}$, $\rho(0) = 1$. When Σ_P is very large, i.e., $\Sigma_P \gg 1$, since $E_{K\text{-}R} \approx E_{K\text{-}L} 2\Sigma_A/\Sigma_P$, which,

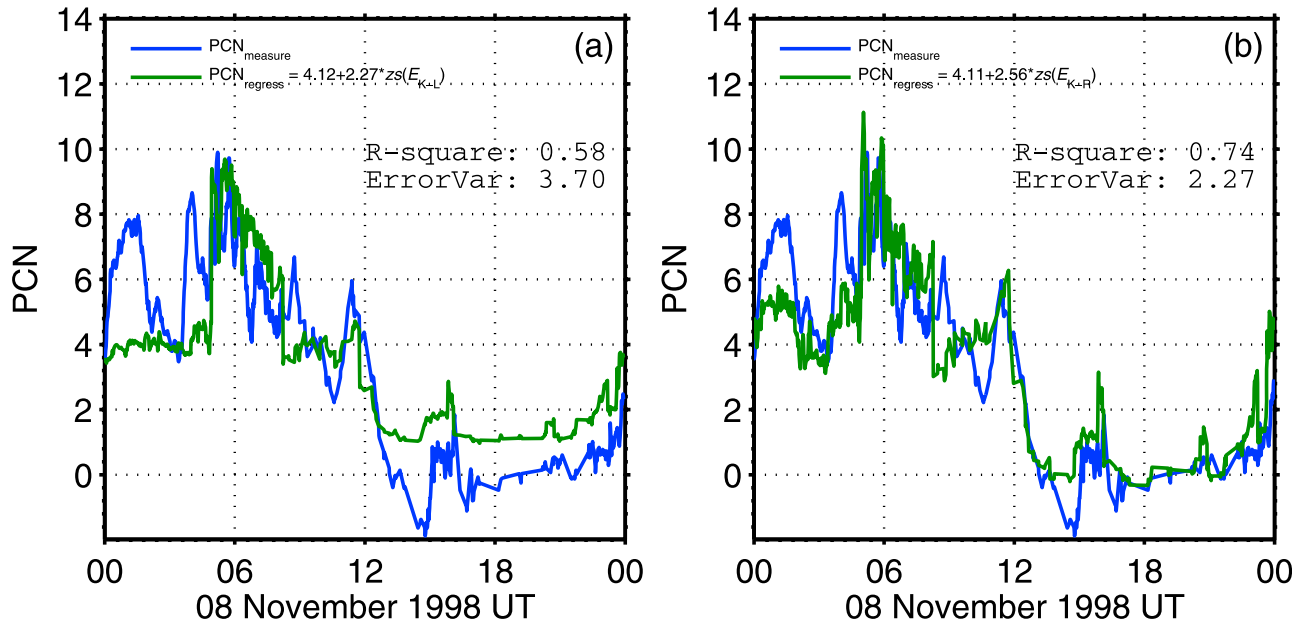

Figure 3. As for Figure 2 for a different event on 8 November 1998.

apart from constant coefficient $2/\Sigma_P$, is equivalent to $E_{K\text{-}L}\Sigma_A$, we have

$$\rho \approx \rho(E_{K\text{-}L}, E_{K\text{-}L}\Sigma_A), \text{when } \Sigma_P \gg 1. \quad (25)$$

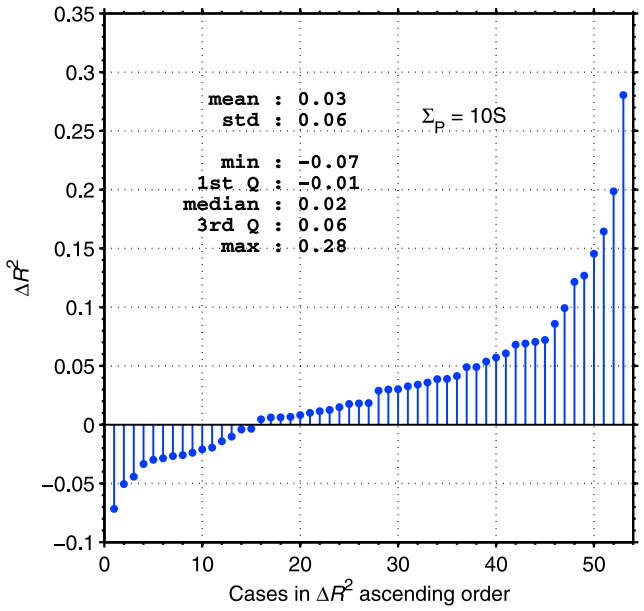

Figure 4. The difference of R^2 (i.e., ΔR^2 defined in equation (22)) when $E_{K\text{-}R}$ is evaluated for Σ_P = 10S for all the 53 cases. The summary statistics are: mean: 0.03; standard deviation: 0.06; minimum: −0.07; 1st quartile: −0.01; median: 0.02; 3rd quartile: 0.06; maximum: 0.28. Cases are arranged in such an order that ΔR^2 increases from left to right. Positive values indicate that by switching from $E_{K\text{-}L}$ to $E_{K\text{-}R}$, the consistency between the measured PCN index and the predicted PCN index is improved. Negative values mean otherwise.

This value of ρ is expected to be smaller than 1. An example of ρ varying as a function of Σ_P on 20 November 2003 is shown in Figure 5. In the range of probable conductance near 10S, the correlation coefficient between $E_{K\text{-}L}$ and $E_{K\text{-}R}$ is 0.92, 0.86, and 0.72 when Σ_P is 5S, 10S, and 15S respectively.

[29] Unlike $\rho(\Sigma_P)$, ΔR^2 (equation (22)), also taken as a function of Σ_P, i.e., $\Delta R^2(\Sigma_P)$, need not change monotonically with Σ_P. An example, again for the case of

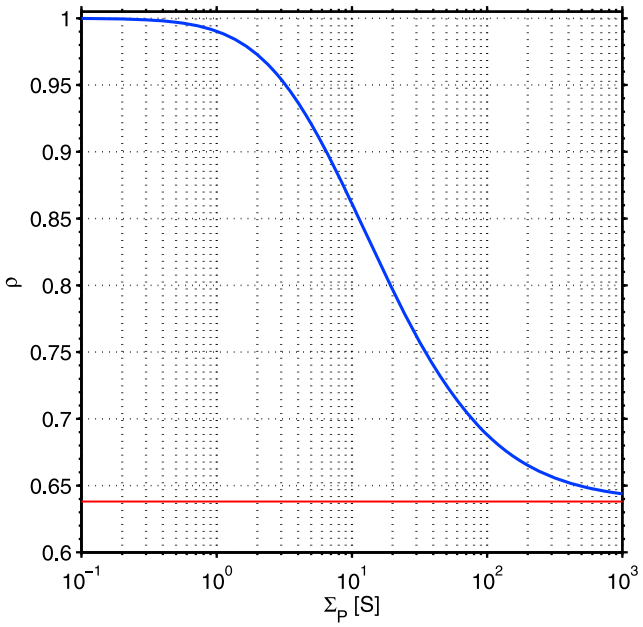

Figure 5. The correlation coefficient between $E_{K\text{-}L}$ and $E_{K\text{-}R}$ (i.e., ρ defined in equation (24)) on 20 November 2003 when $E_{K\text{-}R}$ is evaluated with different values of Σ_P. The red line represents the limit of ρ as Σ_P approaches ∞. The X axis is logarithmic.

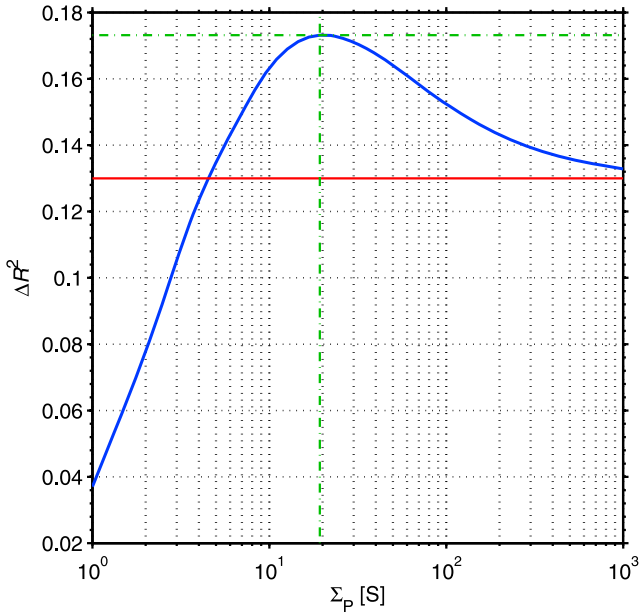

Figure 6. Change of R^2 (i.e., ΔR^2 defined in equation (22)) on 20 November 2003 when $E_{K\text{-}R}$ is evaluated with different values of Σ_P. The blue line represents ΔR^2 as a function of Σ_P. The red line represents the asymptotic value for infinite conductance, $\Delta R^2(\infty)$. The green line gives the maximum value of ΔR^2 and the corresponding Σ_P of 20S. The X axis is logarithmic.

20 November 2003, is shown in Figure 6. The blue line represents ΔR^2 as a function of Σ_P. The green line identifies the maximum ΔR^2, which is 0.175 for Σ_P of 20 S. Although not shown, $\Delta R^2(0) = 0$. As Σ_P approaches ∞, ΔR^2 represents the change of R^2 by switching from $E_{K\text{-}L}$ to $E_{K\text{-}L}\Sigma_A$, which is shown with the red line. As can be seen from Figure 6, ΔR^2 varies over a fairly large range for $\Sigma_P \in [0, \infty)$. However, in reality, Σ_P varies over a small range compared to $[0, \infty)$. Thus, in the following analysis, we concentrate on a subset of $[0, \infty)$ containing only reasonable values of Σ_P.

[30] In order to estimate the range of interest, we use the formula of *Robinson and Vondrak* [1984] which tells us that the Pedersen conductance caused by solar illumination can be estimated as

$$\Sigma_P = C_0 (F_{10.7})^{1/2}, \tag{26}$$

where $F_{10.7}$ represents the strength of 10.7 cm solar radio flux at the Earth and, as recommended by *Ober et al.* [2003], $C_0 = 0.77$. The resulting time series of Σ_P with 1-day resolution from 1 January 1997 to 31 December 2008 is shown in Figure 7a. The corresponding histogram is displayed in Figure 7b. From Figure 7, all of the values lie between 5S and 15S, i.e., $\Sigma_P \in$ [5S, 15S]. By assuming Σ_P = 5S and 15S, the changes of R^2 by switching from $E_{K\text{-}L}$ to $E_{K\text{-}R}$ as solar wind driver are shown in Figures 8a and 8b, respectively. The cases are arranged in the same order as that of Figure 4. Compared with Figure 4, one can see that if R^2 increases by switching from $E_{K\text{-}L}$ to $E_{K\text{-}R}$ for Σ_P = 10S, then it is likely that R^2 increases for $\Sigma_P \in$ [5S, 15S], although the change of ΔR^2 is usually larger for large Σ_P. Thus, $E_{K\text{-}R}$ seems to serve as a potentially better indicator of the solar wind influence on the ionospheric processes than $E_{K\text{-}L}$, and results are plausible for a reasonable range of realistic values of Σ_P. Furthermore, as suggested by *Kivelson and Ridley* [2008], we take 10S as a reasonable estimation of Σ_P in this study as the predictions appear to be little affected by the specific value used in the analysis.

3.3. Internal Driving of the Polar Cap Dynamics

[31] The PCN index is a measure of the magnetic field perturbation at Qaanaaq [*Troshichev et al.*, 1988], and magnetic field perturbations may arise from external driving, e.g., dayside reconnection or viscous interactions between the solar wind and magnetosphere at the low latitude boundary layer [e.g., *Axford*, 1964], and internal driving, e.g., energy release during magnetotail activity, such as substorms. In this

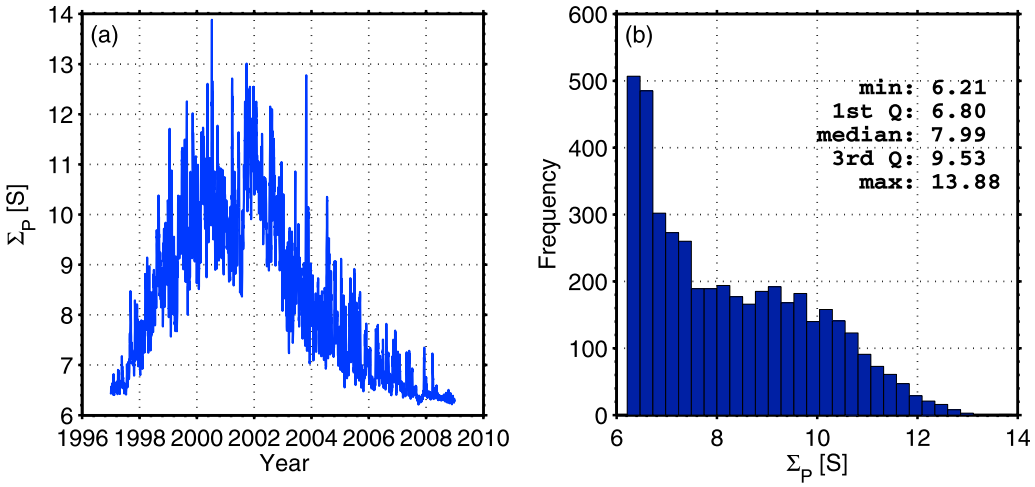

Figure 7. Ionospheric Pedersen conductance, Σ_P, computed by using equation (26) with C_0 = 0.77. (a) Time series of Σ_P from 1 January 1997 to 31 December 2008. (b) The histogram of Σ_P from 1 January 1997 to 31 December 2008 with summary statistics: minimum: 6.21; first quartile: 6.80; median: 7.99; third quartile: 9.53; maximum: 13.88.

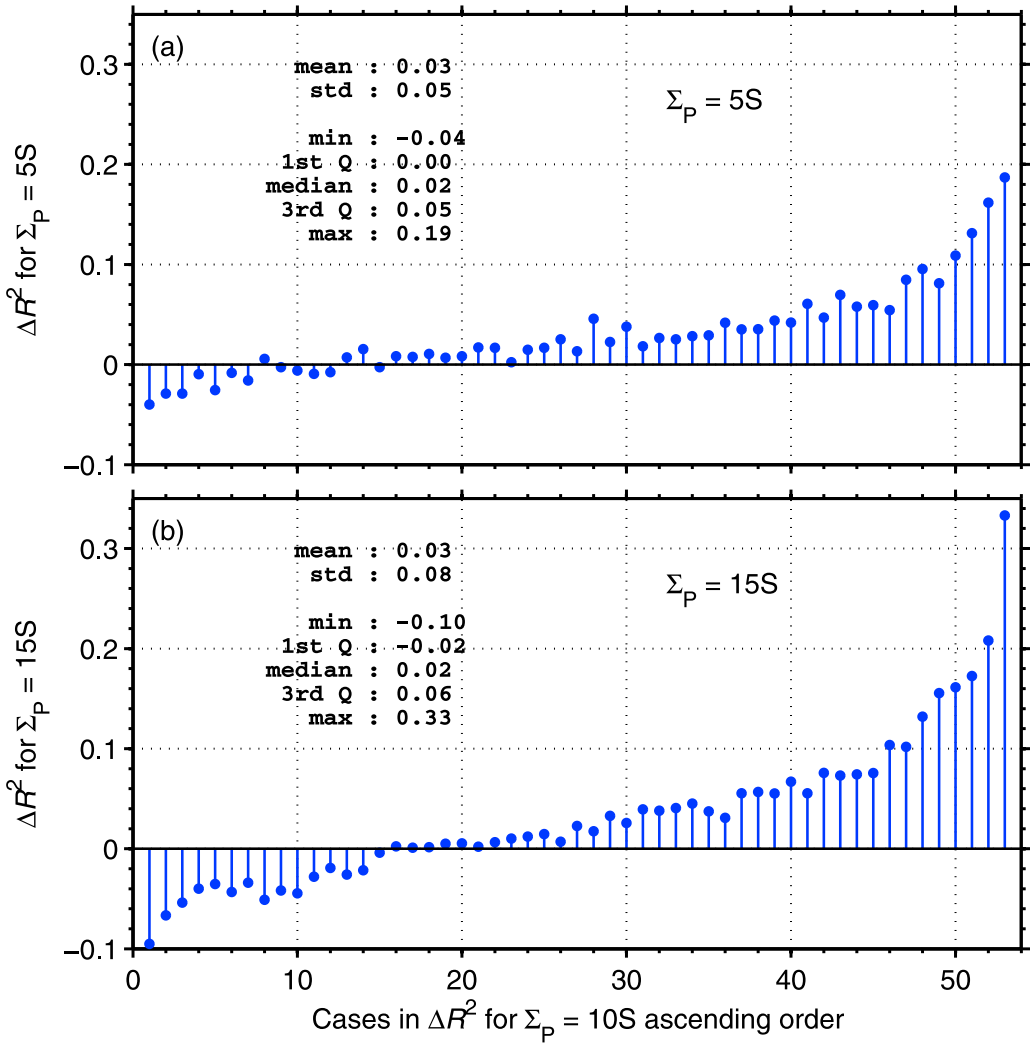

Figure 8. As for Figure 4 for (a) Σ_P = 5S and (b) 15S. The change of R^2 (equation (22)) for Σ_P = 5S is summarized as: minimum: −0.04; 1st quartile: 0.00; median: 0.02; 3rd quartile: 0.05; maximum: 0.19. For Σ_P = 15S, the change of R^2 is summarized as: minimum: −0.10; 1st quartile: −0.02; median: 0.02; 3rd quartile: 0.06; maximum: 0.33. In both panels, cases are in the same order as that of Figure 4.

study, we pay primary attention to dayside reconnection and magnetotail activity, while treating other sources as unexplained errors. According to the principle of superposition, we linearly combine these sources and get

$$\delta B = \delta B_D + \delta B_U + \delta B_O, \tag{27}$$

where δB_D is the magnetic field perturbation at Qaanaaq directly driven by dayside reconnection, δB_U is the magnetic field perturbation at Qaanaaq arising from the energy release in the magnetotail and δB_O represents the other contributions to the magnetic field perturbations at Qaanaaq. In this study, δB_O is attributed to unexplained error. So the equation that we employ is

$$\delta B \approx \delta B_D + \delta B_U. \tag{28}$$

While this greatly simplifies the analysis, it leaves opportunities for improvement in future studies that can consider other sources that can be precisely identified and reasonably modeled. As discussed in section 3.1, we use $E_{K\text{-}R}$ to represent the driving of the solar wind. Thus, as a first order approximation, we assumed a linear dependence between δB_D and $E_{K\text{-}R}$, i.e.,

$$\delta B_D \propto E_{K\text{-}R}. \tag{29}$$

Following *McPherron and Baker* [1993], we use the AL index to represent the contribution of nightside energy release. Figure 9 shows scatterplots among the PCN index, $E_{K\text{-}L}$, $E_{K\text{-}R}$ and the AL index on 20 November 2003 in a matrix form. For example, the 1st row 2nd column is a scatterplot of $E_{K\text{-}L}$ and the PCN index. The better correlation between the PCN index and $E_{K\text{-}R}$ than between the PCN index and $E_{K\text{-}L}$ is evident in row 1 that shows smaller scatter in column 3 than in column 2. This is further confirmed by the better consistency between the original and the flipped scatterplots, i.e., PCN versus $E_{K\text{-}R}$, (row 1, column 3) and $E_{K\text{-}R}$ versus PCN (row 3, column 1) than the pair between PCN and $E_{K\text{-}L}$. Similarly, a better correlation between $E_{K\text{-}R}$

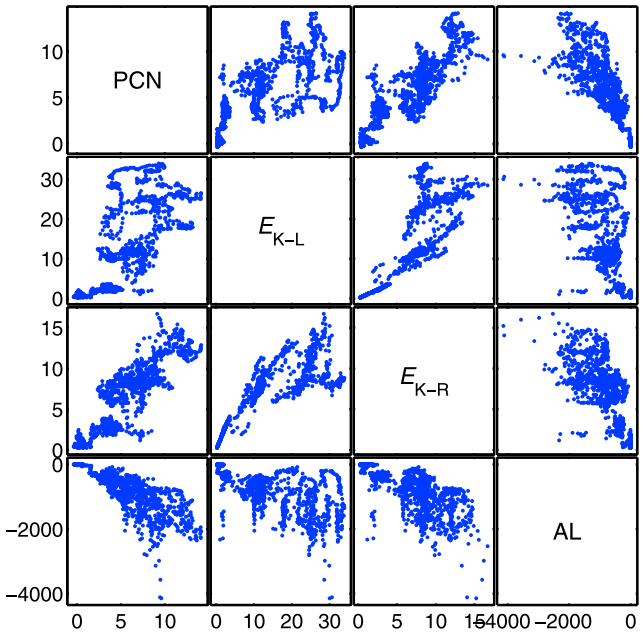

Figure 9. Scatterplot matrix between the measured PCN index, $E_{K\text{-}L}$, $E_{K\text{-}R}$, and the AL index on 20 November 2003. The PCN index is the ordinate of all the plots in 1st row and the abscissa of all the plots in 1st column, etc.

and AL than between $E_{K\text{-}L}$ and AL can be found by comparing row 4 columns 3 and 2. A good correlation between the PCN index and AL (row 4 column 1) is consistent with our choice of AL index as an independent variable when predicting the PCN index from nightside processes.

[32] As our intention is to identify the effects of activity initiated on the nightside of the magnetosphere, it is desirable to remove the portion of AL that responds directly to the solar wind input [*Bargatze et al.*, 1985; *McPherron and Baker*, 1993]. For this reason, we introduce a modified AL parameter, AL_U, defined as follows. We run a regression analysis with AL as the dependent variable and $E_{K\text{-}R}$ as the independent variable for our events to obtain the directly driven portion of AL [*Akasofu*, 1979b; *McPherron and Baker*, 1993], which we define as

$$AL_D = \alpha_0 + \alpha_1 E_{K\text{-}R}, \tag{30}$$

where α_0 and α_1 are regression coefficients. The driven portion of AL is estimated through the R^2 of equation (30) and is shown in Figure 10. On average AL_D contributes 35% of AL for the 53 cases. Then we subtract AL_D from AL to get AL_U, a quantity that is dominated by magnetotail activity [*Akasofu*, 1979b; *McPherron and Baker*, 1993]. Here

$$AL_U = AL - AL_D \tag{31}$$

and, similar to $E_{K\text{-}R}$, a first order approximation is assumed, i.e.,

$$\delta B_U \propto AL_U. \tag{32}$$

A linear regression model that includes both the influence of direct solar wind driving and the influence of nightside energy release on the PCN index can be expressed in terms of the z-score of the two variables in the form

$$PCN_{regress} = \beta_0 + \beta_1 zs(E_{K\text{-}R}) + \beta_2 zs(AL_U), \tag{33}$$

where β_0, β_1 and β_2 are regression coefficients. Note that in equation (33) we use only the portion of the AL index that remains after the effects of $E_{K\text{-}R}$ are removed. *Gao et al.* [2012a] compared the results of the linear model (equation (33)) with those obtained from a more general, nonlinear model, referred to as the additive model, which relates PCN to $E_{K\text{-}R}$ and AL_U through

$$PCN_{additive} = \alpha + f_1(E_{K\text{-}R}) + f_2(AL_U), \tag{34}$$

where α is the intercept, $f_1(\cdot)$ and $f_2(\cdot)$ are arbitrary continuous functions. They found that, in general, the results of the two models are very similar, indicating that the linear approximation is generally valid.

[33] Usually, regression is used to investigate the association of the independent variables and the dependent variable. In the framework of a magnetospheric convection model, the associations between $E_{K\text{-}R}$ and PCN and between AL_U and PCN imply causation ($E_{K\text{-}R}$ drives ionospheric flows that partially control PCN and AL_U drives flows that partially control PCN). For the purpose of establishing the relative importance of the two controlling factors, it is essential to make $E_{K\text{-}R}$ and AL_U dimensionless by replacing them with their corresponding z-scores (equation (19)) as we have done. Figure 11 shows the effect of the AL index on the prediction of the PCN index for the day plotted in Figure 2

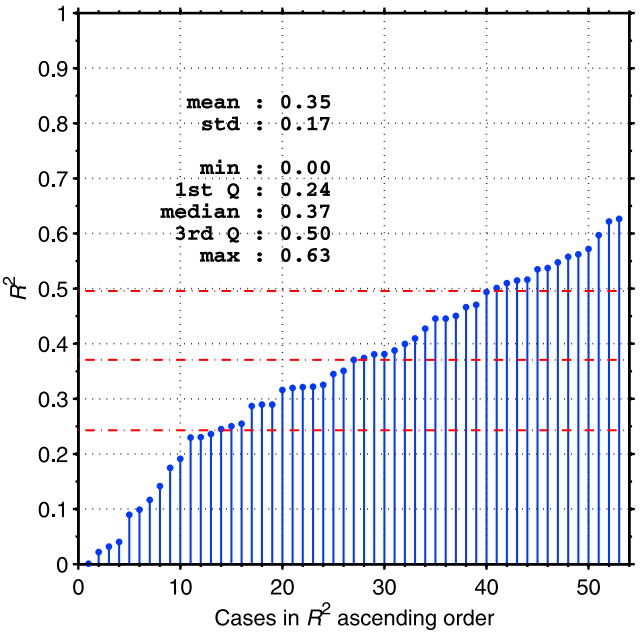

Figure 10. The driven component of AL for the 53 cases estimated through the R^2 of regression between AL and $E_{K\text{-}R}$, i.e., R^2 of equation (30), in R^2 ascending order. The summary statistics are: minimum 0.00; 1st quartile 0.24; median 0.37; 3rd quartile 0.50; maximum 0.63. The mean is 0.35. The red dashed lines are 1st quartile, median and 3rd quartile from bottom to top.

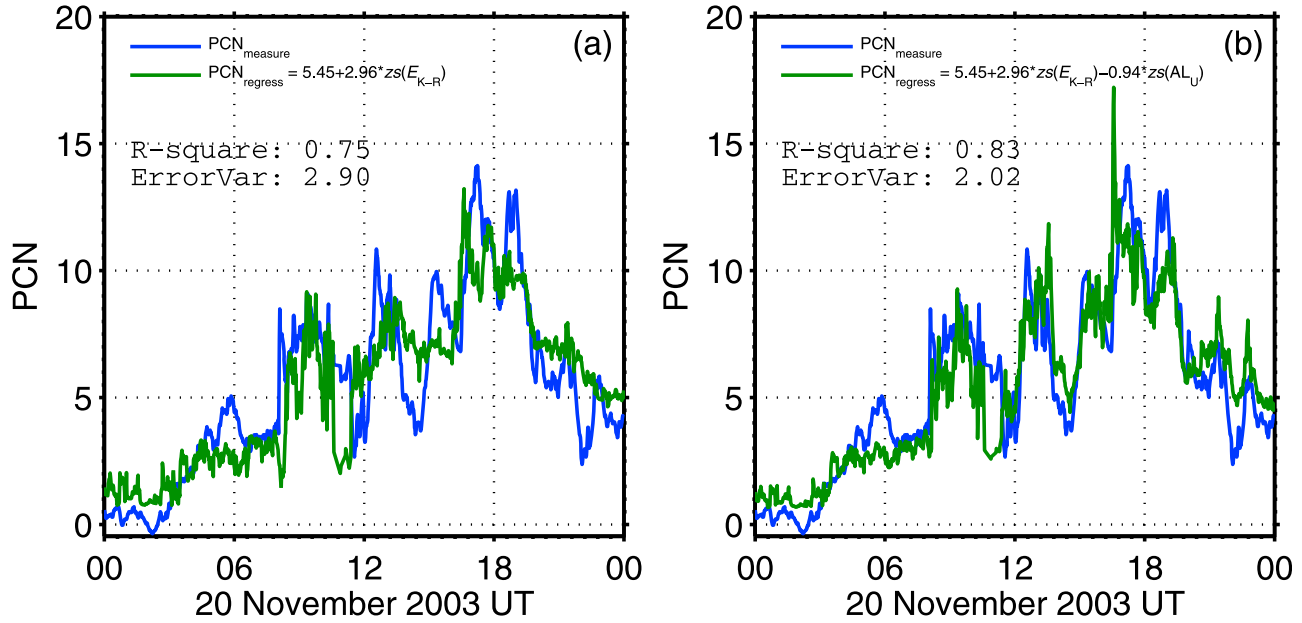

Figure 11. The same day as that plotted in Figure 2 (20 November 2003) (a) without dependence on the AL_U index and (b) with dependence on the AL_U index. The blue lines are the measured PCN index and the green lines are the predicted PCN index. Additional time shift has been added to the propagated solar wind data to achieve the highest correlation between PCN and $E_{K\text{-}R}$.

(20 November 2003). Figure 11a compares the measured PCN index with the predicted PCN index using $E_{K\text{-}R}$ to represent the contributions directly driven by the solar wind. In Figure 11b, we use the formulation of equation (33) including both $E_{K\text{-}R}$ and AL_U as independent variables and find that it improves the consistency between observation and regression, especially at high levels of activity. The addition of a dependence on AL_U increases R^2 from 0.75 to 0.83 and reduces the error variance from 2.90 to 2.02. Figures 12, 13, and 14 apply the same type of analysis to another three cases on 8 November 1998, 22 September 1999 and 7 January 2005. In all cases, it is apparent from the plots that by including a dependence on AL_U, the predictions are improved, especially for PCN > 5. In the additional three cases illustrated, the R^2 increases (0.74 to 0.84, 0.71 to 0.84, and 0.74 to 0.90) and the error variance decreases (2.27 to 1.44, 0.98 to 0.55, and 0.79 to 0.32) significantly when AL_U is added as an independent variable.

[34] Although nightside processes contribute to the PCN index, effects directly driven by dayside reconnection are more important. Since both $E_{K\text{-}R}$ and AL_U are normalized by representing them in terms of their z-scores, a direct

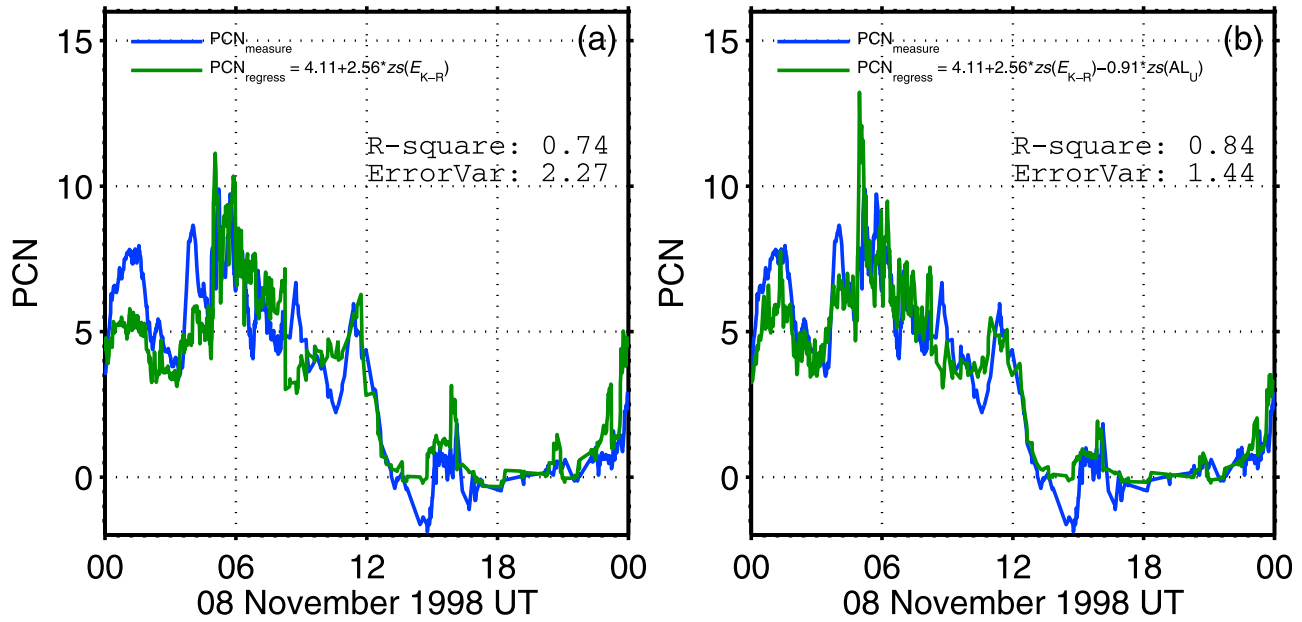

Figure 12. As for Figure 11 for a different event on 8 November 1998 (also in Figure 3).

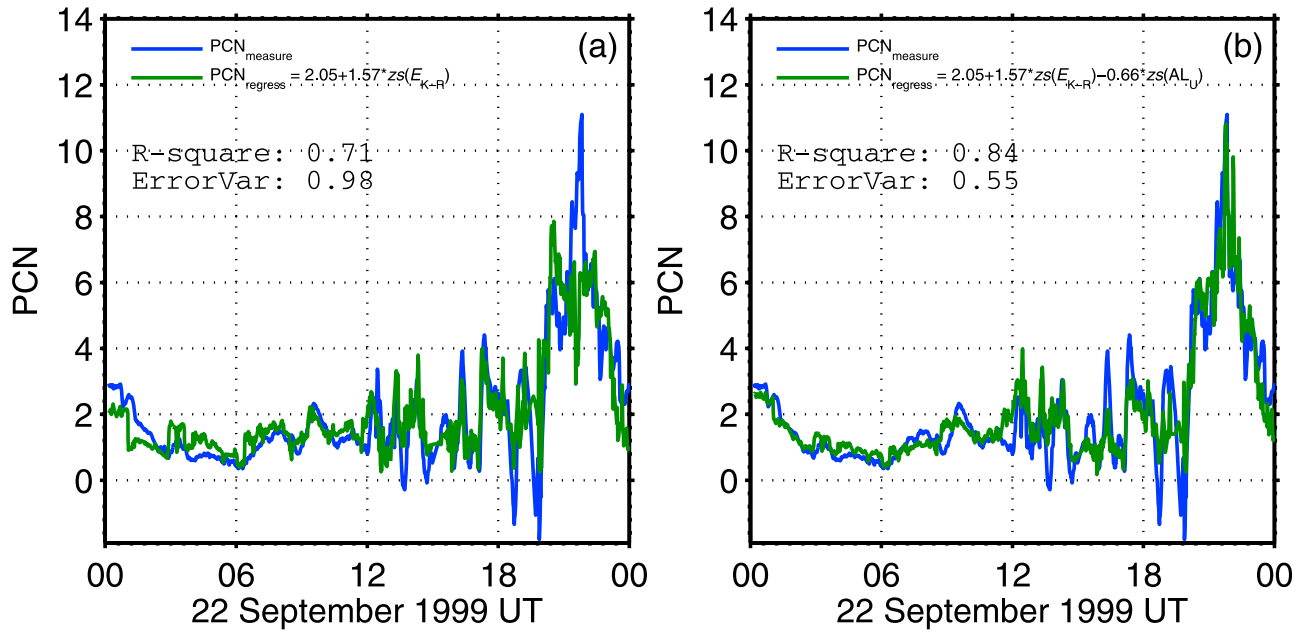

Figure 13. As for Figure 11 for a different event on 22 September 1999.

comparison of the regression coefficients can reveal their relative contributions to the PCN index. Figure 15a shows a scatterplot between the regression coefficients of $E_{K\text{-}R}$ and AL_U for the events with $R^2 \geq 0.5$. The points have been sized and colored according to their R^2 values. If the two input parameters contributed equally to the fit, the points would lie close to the line $y = x$. We perform an orthogonal least squares fit through the origin whose slope reveals the relative magnitudes of β_1 and β_2, i.e., $|\beta_2/\beta_1|$. The best fit gives $y = 0.47x$, indicating that, on average,

$$|\beta_1| \approx 2|\beta_2|. \tag{35}$$

In other words, the directly driven dayside contribution dominates the PCN index by roughly 2:1. This ratio has been confirmed by applying the same analysis to PCS.

[35] As stated in section 3.1, in equation (33), $E_{K\text{-}R}$ is calculated by using the propagated solar wind data with extra time shifts to achieve maximum correlation between $E_{K\text{-}R}$ and PCN. In addition, we use the same $E_{K\text{-}R}$ in equation (30) to derive AL_U. In principle, time delays between AL and $E_{K\text{-}R}$ should also be taken into account. *Bargatze et al.* [1985] studied the temporal relationship between the solar wind and magnetospheric activity by constructing linear prediction filters between uB_s and the AL

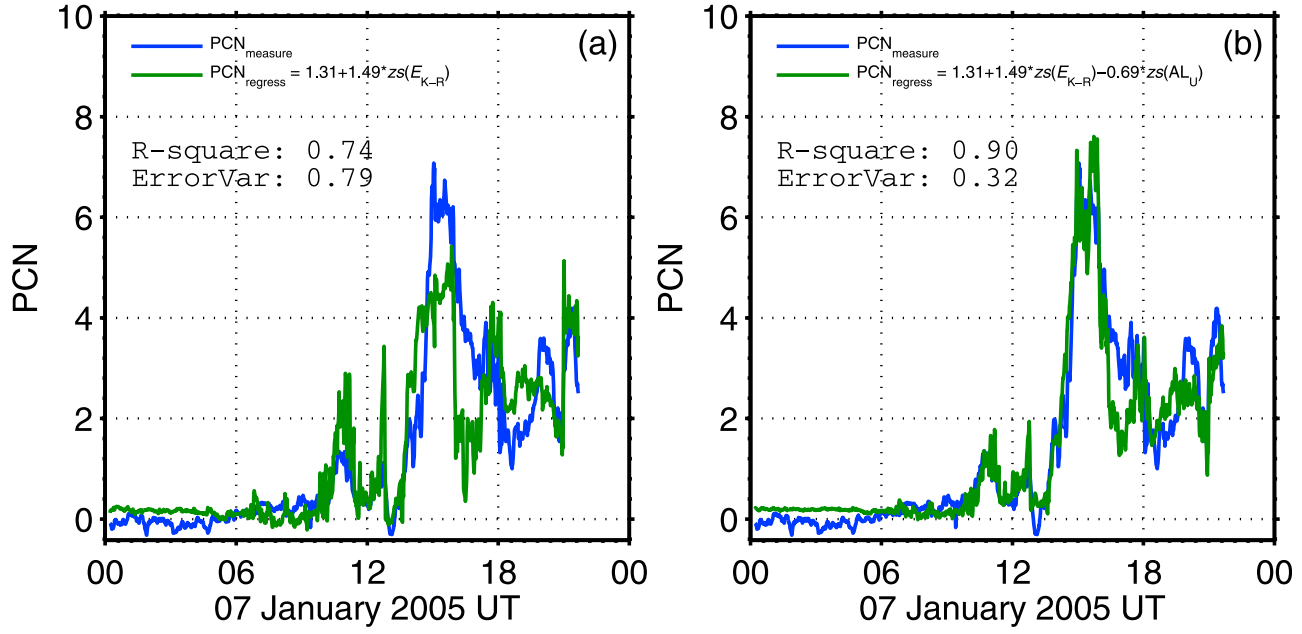

Figure 14. As for Figure 11 for a different event on 7 January 2005.

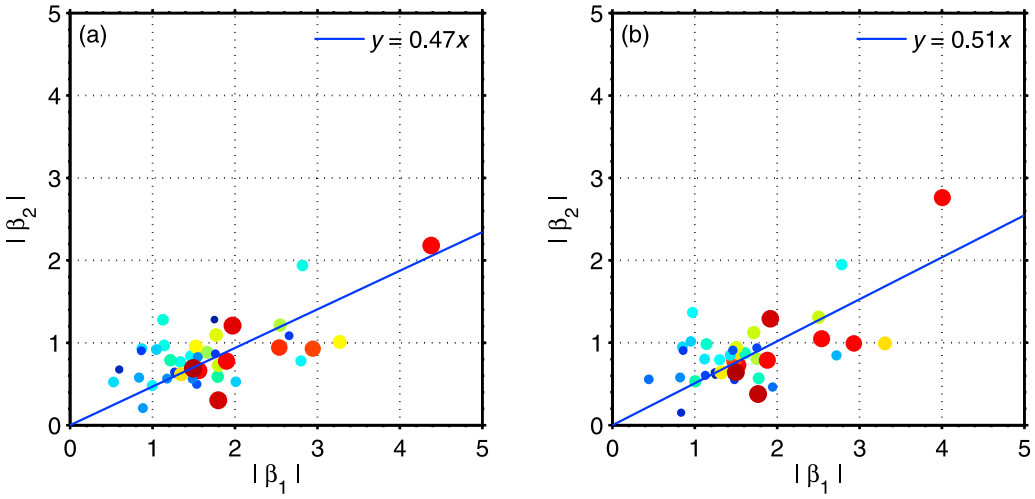

Figure 15. (a) Scatterplot of regression coefficient of AL_U versus regression coefficient of $E_{K\text{-}R}$ for the events with $R^2 \geq 0.5$. The points are both sized and colored according to the R^2 values. The blue line through the origin is an orthogonal least square fit to the points. (b) As for Figure 15a except that an extra 10 min time delay is added to $E_{K\text{-}R}$ when computing AL_U by using equation (30).

index, where u is the solar wind bulk velocity and B_s is related to IMF B_Z through $B_s = -B_Z$ for $B_Z < 0$ and $B_s = 0$, for $B_Z \geq 0$. Using IMP 8 solar wind data propagated to $X_{GSM} = 15R_E$, they found that the filters were composed of two response pulses peaking at time lags 20 and 60 min, and interpreted the 20 min pulse as magnetospheric activity directly driven by the solar wind and the 60 min pulse as response of magnetospheric activity to energy unloading in magnetotail. Following the analysis of *Bargatze et al.* [1985], in order to remove the directly driven component from the AL index, a time delay close to 20 min needs to be added to the propagated solar wind data. Recall that, for each case, we have added a time lag, typically 12 min, to the solar wind data to achieve the highest correlation between PCN and $E_{K\text{-}R}$. Thus, an additional time delay close to 8 min should be added to $E_{K\text{-}R}$ in equation (30). However, with this additional time delay, denoted as $\delta\Delta T$, the results are close to those without it. For example, Figure 16 shows the variations of regression coefficients β_0, β_1, and β_2 for the case of 20 November 2003 with $\delta\Delta T$ varying from -5 to 20 min. From Figure 16, β_0 and β_1 are close to constant for different values of $\delta\Delta T$. β_2 changes from -0.93 to -0.99 when $\delta\Delta T$ varies from 0 to 10 min, and to -1.12 when $\delta\Delta T$ is 20 min. Consequently, the values of the ratio $|\beta_1/\beta_2|$ are 3.16, 2.96, and 2.54 for $\delta\Delta T$ being 0, 10 and 20 min respectively. Thus, although β_0, β_1 and β_2 vary with $\delta\Delta T$, they change little when $\delta\Delta T$ is close to 10 min. In Figure 15b, we show a scatterplot between β_1 and β_2 with an additional time delay of 10 min added to $E_{K\text{-}R}$ when computing AL_U. It is clear that the sizes and colors of the points in Figure 15b are similar to those in Figure 15a, which indicates that the change of R^2 values are small. In fact, if we define the changes of R^2 as

$$\delta R^2 = R^2 \text{ with additional 10 minutes delay} - R^2 \text{ without delay}, \quad (36)$$

then, for our data set, δR^2 is summarized as: minimum: -0.07; 1st quartile: -0.03; median: -0.02; 3rd quartile: -0.06; maximum: 0.04. Thus, by adding additional 10 min delay to $E_{K\text{-}R}$ to compute AL_U, the consistency between the measured PCN and that predicted from equation (33) becomes, on average, slightly worse by 0.02 in terms of R^2. Furthermore, the slope of the fitted line (0.51) is close to that obtained when no extra time delay is added to $E_{K\text{-}R}$ in equation (30) (0.47). Thus, the dayside contribution to the PC index still outweighs the nightside contribution by roughly a factor of 2. In other words, with a time delay close to 10 min added to $E_{K\text{-}R}$ in deriving AL_U, our conclusion remains the same. Although the exact timing between PCN and $E_{K\text{-}R}$ is very important in understanding the details of magnetospheric convection, the conclusions from our analysis are not sensitive to this parameter. Thus, in this paper, we do not introduce an additional time delay in correlating $E_{K\text{-}R}$ with AL. However, this important issue should be addressed in future studies.

[36] In order to test for seasonal variations, we have separated the polar cap index into summer hemisphere and winter hemisphere subsets and calculated contributions from the two sources. For all circumstances examined, the directly driven dayside contribution contributes roughly twice as much to the PC index as the nightside energy release contribution. Since in this study, we have investigated only cases with intense solar wind driving with limited sample size, the seasonal variation, even though it exists, is not likely to be prominent. For a more detailed analysis on seasonal variations, please see *Gao et al.* [2012b].

3.4. Solar Wind Dynamic Pressure Driving of the Polar Cap Dynamics

[37] It has been argued that the PC index responds linearly to a solar wind dynamic pressure pulse, since the change of P_{dyn} alters the magnetopause currents which couple with the ionospheric current system through the Region-1 field-aligned

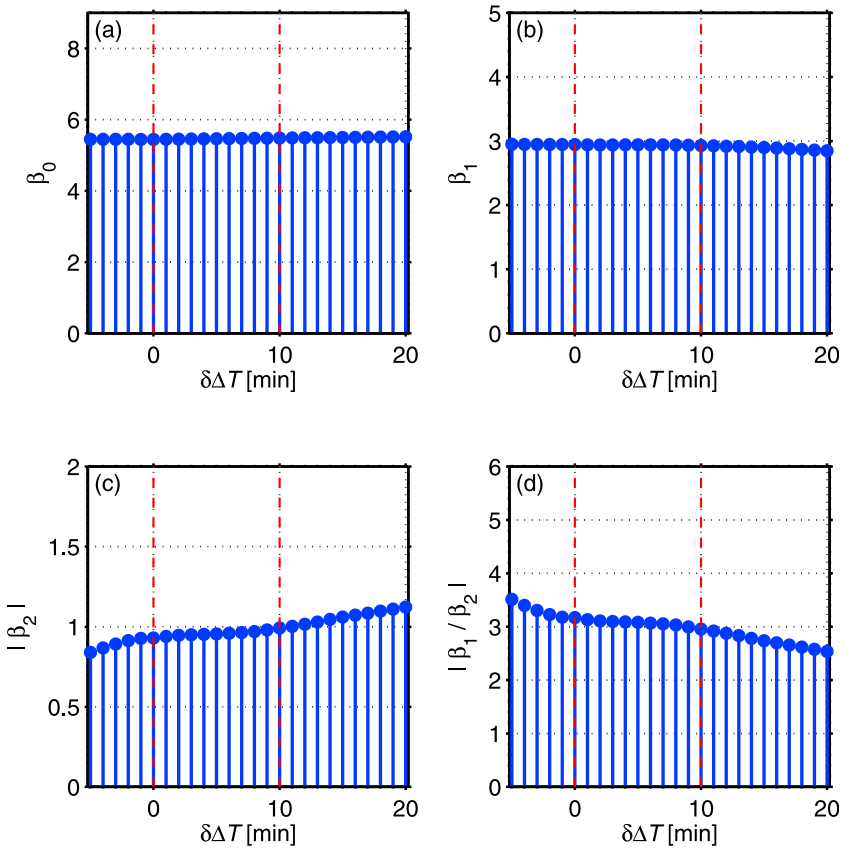

Figure 16. Variations of (a) β_0, (b) β_1, (c) β_2, and (d) $|\beta_1/\beta_2|$ with $\delta\Delta T$ for the case of 20 November 2003. The red dashed lines label $\delta\Delta T = 0$ and 10 min in each panel.

currents and thus change the PC index [e.g., *Stauning and Troshichev*, 2008]. This conclusion has been reached from both case studies [e.g., *Lukianova*, 2003] and statistical analysis [e.g., *Troshichev et al.*, 2007; *Stauning and Troshichev*, 2008]. *Stauning et al.* [2008] studied the dynamic pressure effect for more typical solar wind conditions and found that the PC index responded little to the stationary solar wind dynamic pressure. *Huang* [2005] argued that on average P_{dyn} is a less important contributor to the PC index than the solar wind electric field and substorm activity.

[38] In this study, we use a model selection approach to test the influence of solar wind dynamic pressure on the PCN index with the 53 cases of our study. All the cases are with subintervals during which P_{dyn} changed drastically (e.g., Figure 17a). We propose four models as potential candidates to relate the PCN to solar wind parameters and geomagnetic activity.

$$\text{model}(1): \text{PCN}_{\text{regress}} = \beta_0 + \beta_1 E_{\text{K-R}};$$
$$\text{model}(2): \text{PCN}_{\text{regress}} = \beta_0 + \beta_1 E_{\text{K-R}} + \beta_2 P_{\text{dyn}};$$
$$\text{model}(3): \text{PCN}_{\text{regress}} = \beta_0 + \beta_1 E_{\text{K-R}} + \beta_2 \text{AL}_{\text{U}};$$
$$\text{model}(4): \text{PCN}_{\text{regress}} = \beta_0 + \beta_1 E_{\text{K-R}} + \beta_2 P_{\text{dyn}} + \beta_3 \text{AL}_{\text{U}}{}^*;$$

[39] In model (3), AL_U is calculated from equations (30) and (31), while in model (4) AL_U* is calculated from AL after removing the part that is linearly dependent on both $E_{K\text{-}R}$ and P_{dyn}, i.e., $AL_D{}^* = \alpha_0 + \alpha_1 E_{K\text{-}R} + \alpha_2 P_{dyn}$. Figure 18 shows the changes of R^2 when progressing from model (1) to model (4). We create the figure from a bar plot in which we plot R^2 of model (4) in red, thereafter superposing bars of model (3) in yellow, model (2) in black, and model (1) in white. In Figure 18, the white bars give the R^2 of model (1) for all the 53 cases. The tops of the black bars that are visible above the white bars are the changes of R^2 resulting from switching from model (1) to model (2). Similarly, the parts of the yellow bars that can be seen above the black bars are the additional changes of R^2 resulting from use of model (3) while the parts of the red bars that appear above the yellow bars are the additional changes from use of model (4). The cases are arranged in such an order that R^2 of model (4) increases from left to right. Referring to the visible portions of the different bars, the white bars are the longest, indicating that $E_{K\text{-}R}$ is the most important factor controlling the PCN values. The second longest are the yellow bars, suggesting that AL_U is also a very important factor. The black bars and the red bars represent the effect of P_{dyn} on the PCN and are generally much shorter than the white bars and yellow bars, suggesting that P_{dyn} contributes little to the control of PCN other than through the density variations already accounted for through $E_{K\text{-}R}$ and that it is far less important than $E_{K\text{-}R}$ and AL_U. Thus, in this study, we prefer model (3).

[40] The statistical study of the control of PCN by P_{dyn} shown above can be supplemented by examination of the

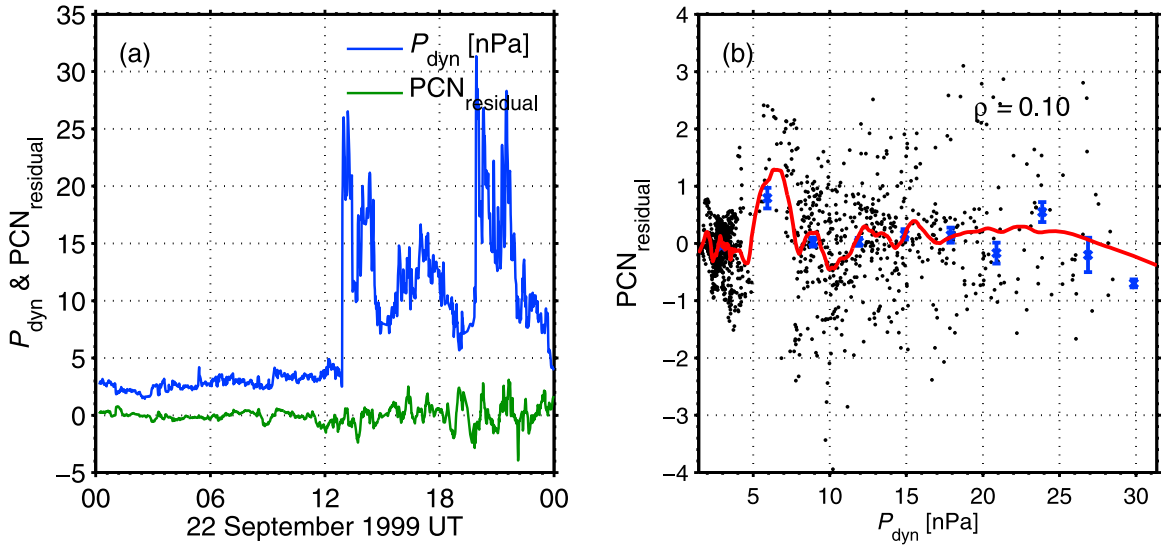

Figure 17. (a) A time series plot of the solar wind dynamic pressure P_{dyn} (blue) and the difference of the measured PCN index and the predicted PCN index, i.e., $PCN_{residual}$ defined in equation (37), (green) on 22 September 1999 (also in Figure 13). (b) Scatterplot between $PCN_{residual}$ and P_{dyn}. The blue crosses indicate the medians in each 2.5 nPa bins. The error bars indicate the errors of the medians. The red line is a running mean of the scatterplot. The correlation coefficient between P_{dyn} and the difference in PCN index for this case is 0.10.

role of P_{dyn} on a case by case basis. An example on 22 September 1999 is shown in Figure 17. In Figure 17a, the time series of solar wind dynamic pressure and the PCN residual, defined as

$$PCN_{residual} = PCN - PCN_{regress}, \quad (37)$$

are plotted versus time. Here $PCN_{regress}$ is the predicted PCN based on model (3). In this case, in which the effect of changing density has been taken into account through its effect on $E_{K\text{-}R}$, there were two jumps of P_{dyn}. At about 1300UT, P_{dyn} jumped from 5 nPa to 25 nPa. At around 2000UT, P_{dyn} increased from less than 10 nPa to over 30 nPa. The PCN residual did not respond to the changes of the solar wind dynamic pressure. Figure 17b shows a scatterplot between P_{dyn} and the PCN residual. The correlation coefficient is only 0.10, and no pattern is identified.

[41] Our data set does include one case in which the PCN index increases concurrently with a jump in P_{dyn} but our model fails to predict the jump. We argue that in this particular case the jump in the PCN index arises because of an unusual excursion of the auroral oval. The event is shown in Figure 19. On 28 April 2001, when P_{dyn} jumped from 0.92 nPa to 13.08 nPa at 0517UT, the PC index increased from 2.05 to 13.76 in the following 20 min. Our model fails to predict the jump of PCN (Figure 20a). In seeking an explanation of the model's failure, we emphasize first that PCN is intended to measure magnetic perturbations on polar cap flux tubes open to the solar wind. A detailed analysis of the aurora using FUV electron data from the Wide-band Imaging Camera (WIC) on the IMAGE satellite [*Mende et al.*, 2000] shows that during the time interval from 0520UT to 0540UT, the auroral oval expanded unusually far poleward to Qaanaaq shown in Figure 20b, the auroral

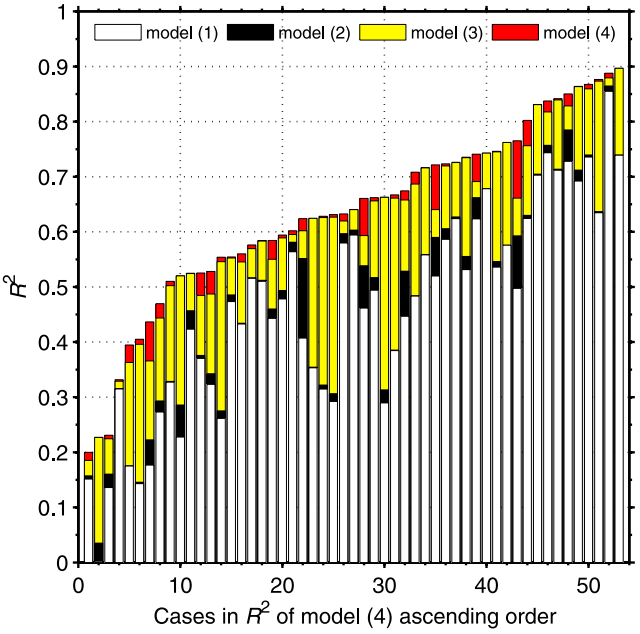

Figure 18. R^2 calculated for model (1), (2), (3) and (4). The construction of the plot is described in the text. White bars indicate the values of R^2 for model (1). The visible portions of the black bars are the changes of R^2 resulting from switching from model (1) to model (2). The portions of the yellow and red bars that are visible in the plot show the changes of R^2 obtained by switching from model (2) to model (3) and from model (3) to model (4) respectively. The cases are arranged in such an order that R^2 of model (4) increases from left to right.

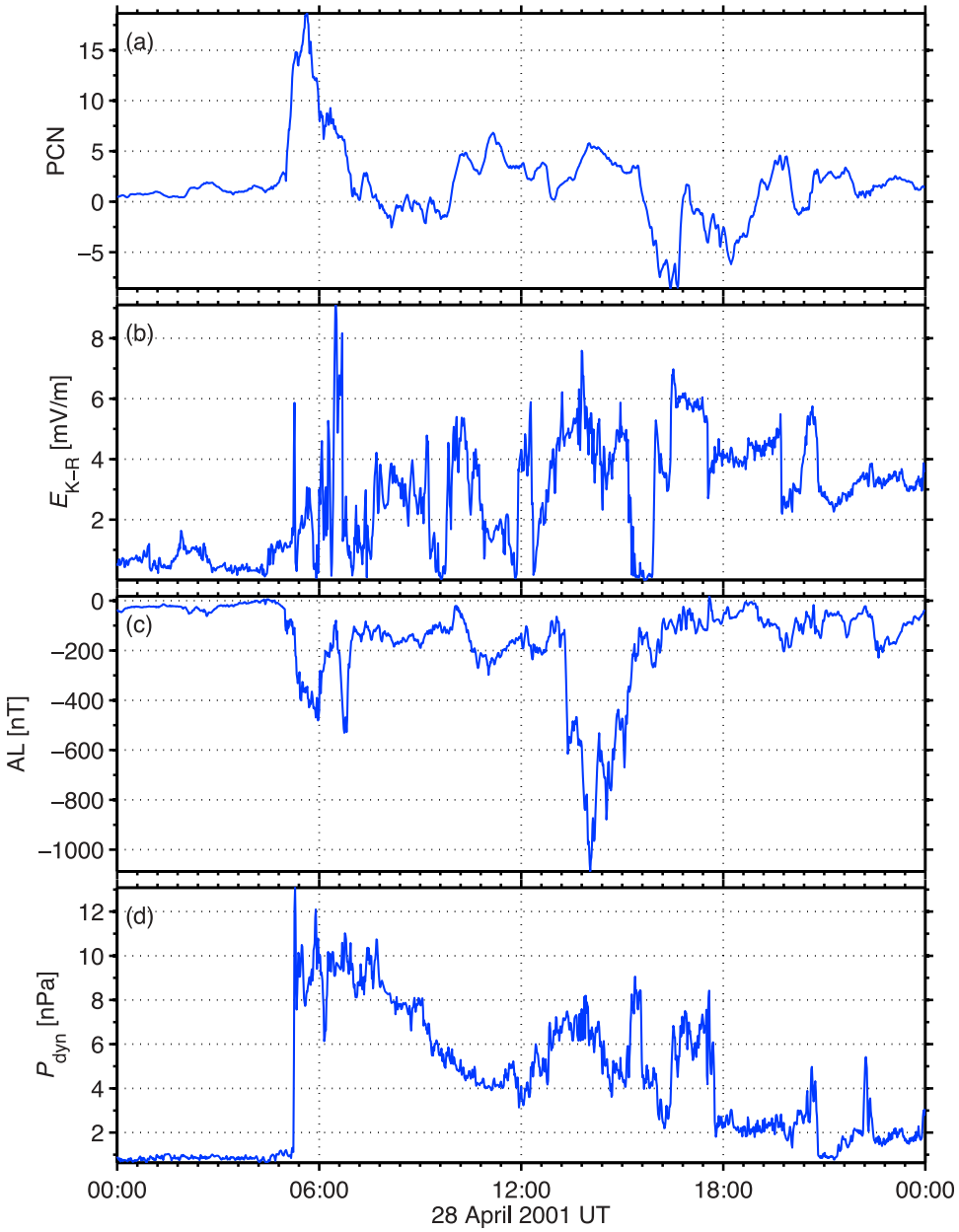

Figure 19. The event of 28 April 2001. Plotted are (a) the PCN index; (b) $E_{K\text{-}R}$; (c) the AL index; and (d) the solar wind dynamic pressure, P_{dyn}. At around 0530UT, P_{dyn} jumped from 2nPa to 14nPa. Almost at the same time, the PCN index increased from 4 to 17.

electrojet moved to unusually high latitudes and it seems that the PCN index recorded perturbations arising from the auroral electrojet. Because of the extreme excursion of the auroral oval, the Qaanaaq station was no longer a polar cap station measuring dominantly the magnetic perturbations on open field lines. Thus, the jump of the PCN index was dominated by local perturbations that overwhelmed any signal directly imposed from the solar wind. We, therefore, attribute the anomalous coincidence between P_{dyn} and the PCN index to the unusual excursion of the aurora during this particular event and argue that it does not imply control of polar cap indices by P_{dyn}.

[42] No clear signature of direct driving of the PCN index by P_{dyn} has been found in our study. We have also tested dP_{dyn}/dt, calculated from differences of consecutive measurements with 1 min resolution, as an independent variable, but still found no evidence of dynamic pressure control of the PCN index.

[43] The fact that correlation between the PCN index and P_{dyn} has been found in previous studies [e.g., *Troshichev et al.*, 2007] can be understood by the following argument. Both $E_{K\text{-}R}$ and P_{dyn} depend on the solar wind number density (n), $\sum_A = 1/\mu_0 v_A \propto n^{1/2}$ and $P_{dyn} \propto n$, and changes of

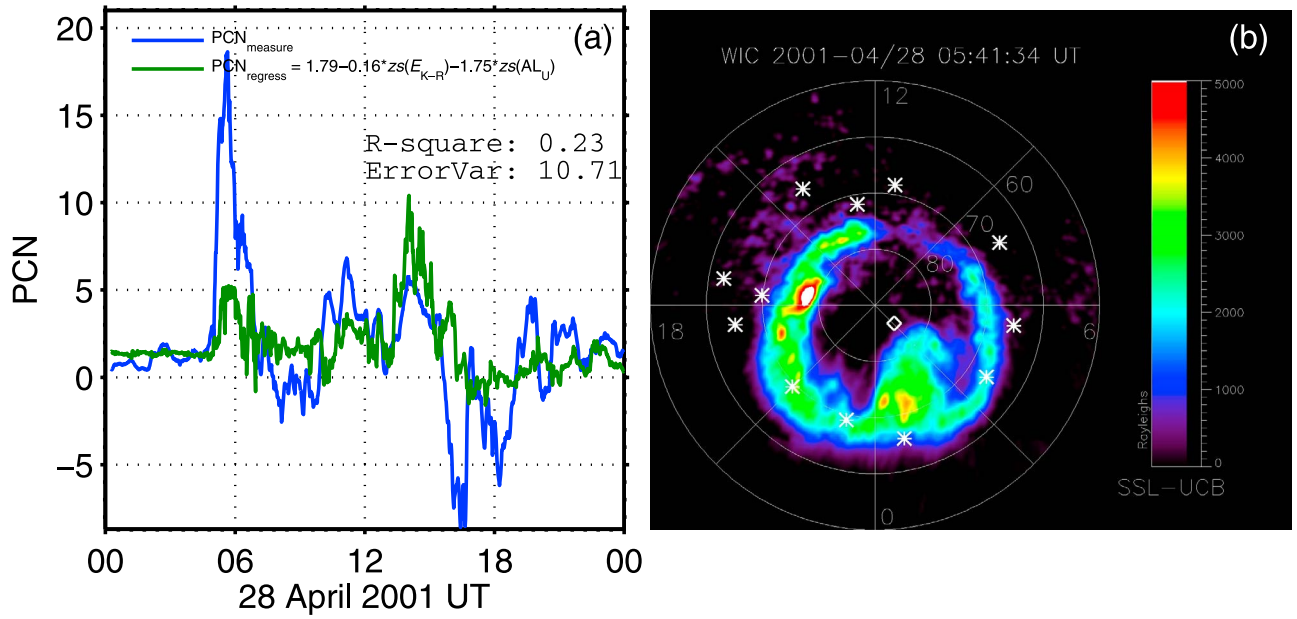

Figure 20. The event of 28 April 2001. (a) The measured PCN index (blue) and the predicted PCN index (green) and (b) The FUV electron auroral oval from WIC/IMAGE at the time 05:41:34UT on 28 April 2001. The vertical white line indicates the noon-midnight meridian, while the horizontal white line is the dawn-dusk meridian. The white concentric circles, centered at the magnetic north pole, are magnetic latitudes separated by 10°. The white crosses locate the AE stations. The diamond near the center shows the location of Qaanaaq.

n result in changes in the PCN index but this effect has been accounted for by the response to $E_{K\text{-}R}$.

3.5. Caveats

[44] Figure 21 shows the sample distribution of R^2 for $E_{K\text{-}R}$ and AL_U as independent variables and the PCN index as a dependent variable. Among our cases, we find general consistency between the measured PCN index and the predicted PCN index obtained from our regression analysis with R^2 typically greater than 0.5, but caveats remain. There are various factors that may cause the model to fail to work such as: (1) The PCN index may take on negative values, but the mechanisms linked to the input parameters that we have considered should not produce negative values of the index. It has been widely accepted that negative PCN is caused by locally sunward convection. In our analysis, we consider indices expected to drive large scale anti-sunward convection at high latitudes. Therefore, when there is an interval with negative PCN, the value predicted by regression analysis will miss it. For example, in Figure 20a, the PCN index becomes negative from 1500UT to 1900UT on 28 April 2001. If we had omitted the data from this time interval, the consistency would have improved. (2) The ionospheric Pedersen conductance Σ_P is crucial to the calculation of the Kivelson-Ridley electric field. However, Σ_P can only be estimated. In this study, we use a crude value of 10S. Although we found that our conclusion holds when using the values 5S and 15S for Σ_P, in a more complete study, it would be worthwhile to improve the estimate of the ionospheric conductance. (3) We use the propagated solar wind data. The propagation technique is crucial to the solar wind data quality. During a time interval when the propagation fails to work, any prediction is likely to fail [*Ridley*, 2000; *Ashour-Abdalla et al.*, 2008]. (4) If the auroral oval expands far poleward to Qaanaaq, the station used may approach the boundary of the polar cap (e.g., Figure 20b) or even cross it. During such intervals, the electrojet may move far from

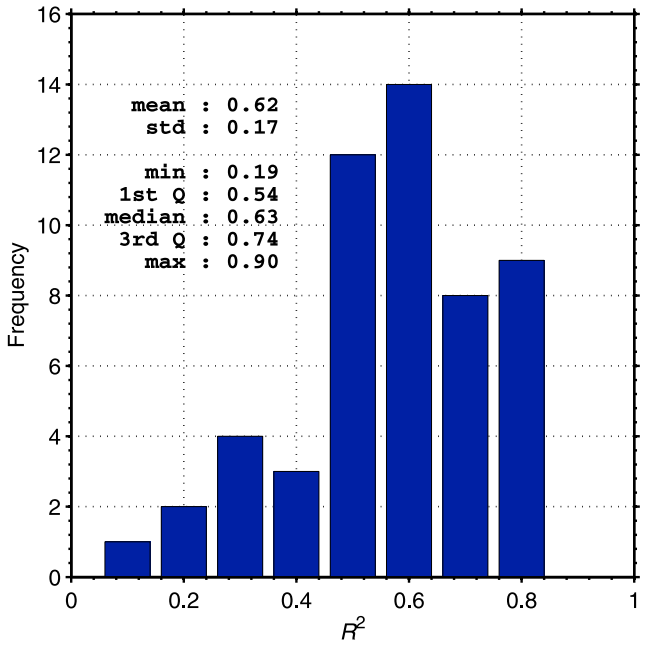

Figure 21. Sample distribution of R^2 with $E_{K\text{-}R}$ and AL_U as independent variables and the PCN index as dependent variable (equation (33)) with summary statistics (mean: 0.62; standard deviation: 0.17; minimum: 0.19; 1st quartile: 0.54; median: 0.63; 3rd quartile: 0.74; maximum: 0.90).

stations used to evaluate AL, and AL may no longer be a good indicator of the nightside processes. In addition, the PCN index will be compromised as a measure of magnetic field perturbations on open field lines. Thus such intervals must be removed from any data set used to interpret the processes nominally measured by the PCN index and by AL. Unfortunately, owing to limited observations of the aurora, we have been able to test only 1 case in which a significant disagreement with the model could be seen to arise because of an anomalous excursion of the auroral electrojet. See *Gao* [2012] for a more detailed discussion of the mechanisms causing the model to fail.

4. Discussion and Conclusions

[45] In this study, we investigated the polar cap dynamics influenced by solar wind input and geomagnetic activity by studying the relationship between the PCN index and solar wind parameters and geomagnetic indices. First, we selected one to two-day intervals within which $E_{\text{K-L}}$ exceeded 10 mV/m. We identified 53 cases from 1998 to 2006 for further study. Then we examined the correlation between the PCN and various solar wind-magnetosphere coupling functions. We found that $E_{\text{K-R}}$, a form representative of the electric field imposed on the ionosphere by magnetopause reconnection that takes saturation into account, serves as a potentially better indicator of the dayside contribution to the polar cap than any previously proposed coupling function between the solar wind and magnetosphere including $E_{\text{K-L}}$ during intervals of high geomagnetic activity. An important parameter in determining $E_{\text{K-R}}$ is the ionospheric Pedersen conductance which can only be poorly estimated. In this paper, we fixed Σ_P at 10S. To test the sensitivity of our conclusion to different values of Σ_P, we performed the same analysis when Σ_P varies within a reasonable range from 5S to 15S. We found that, for a given case, if PCN correlates with $E_{\text{K-R}}$ better than with $E_{\text{K-L}}$ for Σ_P = 10S, then the same conclusion is achieved for $\Sigma_P \in$ [5S, 15S], although the improvements, measured by the increase of R^2, by switching from $E_{\text{K-L}}$ to $E_{\text{K-R}}$ is usually larger when Σ_P takes on larger values.

[46] Taking AL_U (equation (31)) as an indicator of the effects of nightside geomagnetic activity not directly driven by the solar wind electric field, we demonstrated that the PCN index is responsive to that source as well as the solar wind source. The consistency of the measured PCN index and the PCN index predicted from our regression analysis is found to be improved significantly by introducing contributions from AL_U, the part of AL not directly driven. We found that the directly driven part of the AL, i.e., AL_D can explain, on average, 35% of the variation of the AL index, leaving the rest, 65%, controlled by magnetotail activity. Although generally the contribution to PCN from AL_U is less important than the contribution from the modified solar wind electric field ($E_{\text{K-R}}$) in the sense that the regression coefficient of AL_U is smaller than that of $E_{\text{K-R}}$ by a factor of two, they are comparable in magnitude.

[47] We also explored the relationship between the PCN index and the solar wind dynamic pressure. Based on our study, we did not find a clear signature of a direct response of the PCN index to P_{dyn} or jumps in P_{dyn}, if the effect of changing density is modeled by $E_{\text{K-R}}$. One case showed a coincidence between jumps of the PCN and P_{dyn}, but we argued that during this interval the station used for determination of the PCN index was not located well within the polar cap because the auroral oval expanded exceptionally far poleward.

[48] Eventually, we arrived at our model relating the PCN index to solar wind driving ($E_{\text{K-R}}$) and magnetotail energy unloading (AL_U), i.e., equation (33), which is rewritten here for emphasis,

$$\text{PCN} \approx \beta_0 + \beta_1 zs(E_{\text{K-R}}) + \beta_2 zs(\text{AL}_U). \tag{38}$$

Since the polar cap index is measured from only one station for each hemisphere, it cannot give information on the entire polar cap. Nevertheless, the generality of the PC index is justified by its high correlation to other ionospheric quantities, e.g., cross polar cap potential, Joule heating, etc. Thus, similar conclusions are expected if the polar cap dynamics are measured more globally.

[49] **Acknowledgments.** Y. Gao acknowledges support from NASA under grant NNX07AC93G. He appreciates having been given the opportunity to pursue this work during his graduate study at the department of Earth and Space Sciences in University of California, Los Angeles. Y. Gao is grateful to H. U. Frey for generating the aurora plots. He also thanks R. L. McPherron and K. K. Khurana for helpful discussions. The PC index data were obtained from O. A. Troshichev for initial analysis. The PCN data from which the results are reported in this paper were downloaded from ftp://ftp.space.dtu.dk/WDC/indices/pcn. The PCS index data can be downloaded from http://www.aari.nw.ru. The AE index data were obtained from http://wdc.kugi.kyoto-u.ac.jp. The far ultraviolet (FUV) auroral plot from the Wide-band Imaging Camera (WIC) on the IMAGE satellite was analyzed by H. U. Frey at the University of California, Berkeley. The ACE data are propagated by J. M. Weygand using the technique of *Weimer et al.* [2003] and *Weiner* [2004] and are available through Virtual Magnetospheric Observatory (VMO) (http://vmo.igpp.ucla.edu).

[50] Philippa Browning thanks the reviewers for their assistance in evaluating this paper.

References

Akasofu, S. I. (1979a), What is a magnetospheric substorm?, in *Dynamics of Magnetosphere*, edited by S. I. Akasofu, pp. 447–460, D. Reidel, Dordrecht, Netherlands, doi:10.1007/978-94-009-9519-2_23.

Akasofu, S. I. (1979b), Interplanetary energy flux associated with magnetospheric substorms, *Planet. Space Sci.*, *27*, 425–431, doi:10.1016/0032-0633(79)90119-3.

Ashour-Abdalla, M., R. J. Walker, V. Peroomian, and M. El-Alaoui (2008), On the importance of accurate solar wind measurements for studying magnetospheric dynamics, *J. Geophys. Res.*, *113*, A08204, doi:10.1029/2007JA012785.

Axford, W. I. (1964), Viscous interaction between the solar wind and the Earth's magnetosphere, *Planet. Space Sci.*, *12*(1), 45–53, doi:10.1016/0032-0633(64)90067-4.

Bargatze, L. F., D. N. Baker, E. W. Hones Jr., and R. L. McPherron (1985), Magnetospheric impulse response for many levels of geomagnetic activity, *J. Geophys. Res.*, *90*, 6387–6394, doi:10.1029/JA090iA07p06387.

Borovsky, J. E., B. Lavraud, and M. M. Kuznetsova (2009), Polar cap potential saturation, dayside reconnection, and changes to the magnetosphere, *J. Geophys. Res.*, *114*, A03224, doi:10.1029/2009JA014058.

Chun, F. K., D. J. Knipp, M. G. McHarg, G. Lu, B. A. Emery, S. Vennerstrøm, and O. A. Troshichev (1999), Polar cap index as a proxy for hemispheric Joule heating, *Geophys. Res. Lett.*, *26*, 1101–1104, doi:10.1029/1999GL900196.

Chun, F. K., D. J. Knipp, M. G. McHarg, J. R. Lacey, G. Lu, and B. A. Emery (2002), Joule heating patterns as a function of polar cap index, *J. Geophys. Res.*, *107*(A7), 1119, doi:10.1029/2001JA000246.

Fiori, R. A. D., A. V. Koustov, D. Boteler, and R. A. Makarevich (2009), PCN magnetic index and average convection velocity in the polar cap inferred from SuperDARN radar measurements, *J. Geophys. Res.*, *114*, A07225, doi:10.1029/2008JA013964.

Gao, Y. (2012), On anomalous departures from a linear relation between the polar cap index and its controlling factors in solar wind and magnetotail, *J. Geophys. Res.*, *117*, A06201, doi:10.1029/2012JA017721.

Gao, Y., M. G. Kivelson, and R. J. Walker (2012a), The linear dependence of polar cap index on its controlling factors in solar wind and magnetotail, *J. Geophys. Res.*, *117*, A05213, doi:10.1029/2011JA017229..

Gao, Y., M. G. Kivelson, R. J. Walker, and J. M. Weygand (2012b), Long-term variation of driven and unloading effects on polar cap dynamics, *J. Geophys. Res.*, *117*, A02203, doi:10.1029/2011JA017149.

Hill, T. W., A. J. Dessler, and R. A. Wolf (1976), Mercury and Mars: The role of ionospheric conductivity in the acceleration of magnetospheric particles, *Geophys. Res. Lett.*, *3*(8), 429–432, doi:10.1029/GL003i008p00429.

Huang, C.-S. (2005), Variations of polar cap index in response to solar wind changes and magnetospheric substorms, *J. Geophys. Res.*, *110*, A01203, doi:10.1029/2004JA010616.

Iijima, T., and T. Nagata (1972), Signatures for substorm development of the growth phase and expansion phase, *Planet. Space Sci.*, *20*, 1095–1112, doi:10.1016/0032-0633(72)90219-X.

Janzhura, A. S., and O. A. Troshichev (2008), Determination of the running quiet daily geomagnetic variation, *J. Atmos. Terr. Phys.*, *70*(7), 962–972, doi:10.1016/j.jastp.2007.11.004.

Kan, J. R., and L. C. Lee (1979), Energy coupling function and solar wind-magnetosphere dynamo, *Geophys. Res. Lett.*, *6*, 577–580, doi:10.1029/GL006i007p00577.

Kitamura, N., Y. Ogawa, Y. Nishimura, N. Terada, T. Ono, A. Shinbori, A. Kumamoto, V. Truhlik, and J. Smilauer (2011), Solar zenith angle dependence of plasma density and temperature in the polar cap ionosphere and low-altitude magnetosphere during geomagnetically quiet periods at solar maximum, *J. Geophys. Res.*, *116*, A08227, doi:10.1029/2011JA016631.

Kivelson, M. G., and A. J. Ridley (2008), Saturation of the polar cap potential: Inference from Alfvén wing arguments, *J. Geophys. Res.*, *113*, A05214, doi:10.1029/2007JA012302.

Kokubun, S. (1972), Relationship of interplanetary magnetic field structure with development of substorm and storm main phase, *Planet. Space Sci.*, *20*(7), 1033–1049, doi:10.1016/0032-0633(72)90214-0.

Liou, K., J. F. Carbary, P. T. Newell, C.-I. Meng, and O. Rasmussen (2003), Correlation of auroral power with the polar cap index, *J. Geophys. Res.*, *108*(A3), 1108, doi:10.1029/2002JA009556.

Lukianova, R. Y. (2003), Magnetospheric response to sudden changes in solar wind dynamic pressure inferred from polar cap index, *J. Geophys. Res.*, *108*(A12), 1428, doi:10.1029/2002JA009790.

McPherron, R. L., and D. N. Baker (1993), Factors influencing the intensity of magnetospheric substorms, *J. Atmos. Terr. Phys.*, *55*(8), 1091–1122, doi:10.1016/0021-9169(93)90040-6.

Mende, S. B., et al. (2000), Far ultraviolet imaging from the IMAGE spacecraft. 2. Wideband FUV imaging, *Space Sci. Rev.*, *91*(1), 271–285, doi:10.1023/A:1005227915363.

Myers, R. H. (2000), *Classical and Modern Regression With Applications*, 2nd ed., Duxbury, Boston, Mass.

Nagatsuma, T. (2002), Saturation of polar cap potential by intense solar wind electric fields, *Geophys. Res. Lett.*, *29*(10), 1422, doi:10.1029/2001GL014202.

Ober, D. M., N. C. Maynard, and W. J. Burke (2003), Testing the Hill model of transpolar potential saturation, *J. Geophys. Res.*, *108*(A12), 1467, doi:10.1029/2003JA010154.

Pudovkin, M. I., V. V. Lebedeva, and M. F. Heyn (1982), Magnetosheath's parameters and their dependence on intensity and direction of the solar wind magnetic field, *J. Geophys. Res.*, *87*, 8131–8138, doi:10.1029/JA087iA10p08131.

Reiff, P. H., and J. G. Luhmann (1986), Solar wind control of the polar-cap voltage, in *Solar Wind Magnetosphere Coupling*, *Astrophys. Space Sci. Libr.*, vol. 126, edited by Y. Kamide, pp. 453–476, D. Reidel, Dordrecht, Netherlands.

Ridley, A. J. (2000), Estimations of the uncertainty in timing the relationship between magnetospheric and solar wind processes, *J. Atmos. Terr. Phys.*, *62*(9), 757–771, doi:10.1016/S1364-6826(00)00057-2.

Ridley, A. J., and E. A. Kihn (2004), Polar cap index comparisons with AMIE cross polar cap potential, electric field, and polar cap area, *Geophys. Res. Lett.*, *31*, L07801, doi:10.1029/2003GL019113.

Robinson, R. M., and R. R. Vondrak (1984), Measurements of *E* region ionization and conductivity produced by solar illumination at high latitudes, *J. Geophys. Res.*, *89*(A6), 3951–3956, doi:10.1029/JA089iA06p03951.

Russell, C. T., G. Lu, and J. G. Luhmann (2000), Lessons from the ring current injection during the September 24, 25, 1998 storm, *Geophys. Res. Lett.*, *27*(9), 1371–1374, doi:10.1029/1999GL003718.

Shepherd, S. G., R. A. Greenwald, and J. M. Ruohoniemi (2002), Cross polar cap potentials measured with Super Dual Auroral Radar Network during quasi-steady solar wind and interplanetary magnetic field conditions, *J. Geophys. Res.*, *107*(A7), 1094, doi:10.1029/2001JA000152.

Siscoe, G. L., G. M. Erickson, B. U. Ö. Sonnerup, N. C. Maynard, J. A. Schoendorf, K. D. Siebert, D. R. Weimer, W. W. White, and G. R. Wilson (2002), Hill model of transpolar potential saturation: Comparisons with MHD simulations, *J. Geophys. Res.*, *107*(A6), 1075, doi:10.1029/2001JA000109.

Siscoe, G. L., J. Raeder, and A. J. Ridley (2004), Transpolar potential saturation models compared, *J. Geophys. Res.*, *109*, A09203, doi:10.1029/2003JA010318.

Stauning, P. (2011), Comment on "The PC index: Review of methods", by McCreadie and Menvielle (2010), *Ann. Geophys.*, *29*(6), 1137–1146, doi:10.5194/angeo-29-1137-2011.

Stauning, P., and O. A. Troshichev (2008), Polar cap convection and PC index during sudden changes in solar wind dynamic pressure, *J. Geophys. Res.*, *113*, A08227, doi:10.1029/2007JA012783.

Stauning, P., O. Troshichev, and A. Janzhura (2008), The polar cap (PC) indices: Relations to solar wind parameters and global magnetic activity, *J. Atmos. Terr. Phys.*, *70*, 2246–2261, doi:10.1016/j.jastp.2008.09.028.

Troshichev, O. A., and R. Y. Lukianova (2002), Relation of PC index to the solar wind parameters and substorm activity in time of magnetic storms, *J. Atmos. Terr. Phys.*, *64*, 585–591, doi:10.1016/S1364-6826(02)00016-0.

Troshichev, O. A., V. G. Andrezen, S. Vennerstrøm, and E. Friis-Christensen (1988), Magnetic activity in the polar cap—A new index, *Planet. Space Sci.*, *36*, 1095–1102, doi:10.1016/0032-0633(88)90063-3.

Troshichev, O. A., H. Hayakawa, A. Matsuoka, T. Mukai, and K. Tsuruda (1996), Cross polar cap diameter and voltage as a function of PC index and interplanetary quantities, *J. Geophys. Res.*, *101*, 13,429–13,435, doi:10.1029/95JA03672.

Troshichev, O. A., R. Y. Lukianova, V. O. Papitashvili, F. J. Rich, and O. Rasmussen (2000), Polar cap index (PC) as a proxy for ionospheric electric field in the near-pole region, *Geophys. Res. Lett.*, *27*, 3809–3812, doi:10.1029/2000GL003756.

Troshichev, O. A., A. Janzhura, and P. Stauning (2006), Unified PCN and PCS indices: Method of calculation, physical sense, and dependence on the IMF azimuthal and northward components, *J. Geophys. Res.*, *111*, A05208, doi:10.1029/2005JA011402.

Troshichev, O. A., A. S. Janzhura, and P. Stauning (2007), Magnetic activity in the polar caps: Relation to sudden changes in the solar wind dynamic pressure, *J. Geophys. Res.*, *112*, A11202, doi:10.1029/2007JA012369.

Vennerstrøm, S. (1991), The geomagnetic activity index PC, PhD thesis, 105 pp., Dan. Meteorol. Inst., Copenhagen.

Vennerstrøm, S., E. Friis-Christensen, O. A. Troshichev, and V. G. Andresen (1991), Comparison between the polar cap index, *PC*, and the auroral electrojet indices *AE*, *AL*, and *AU*, *J. Geophys. Res.*, *96*, 101–113, doi:10.1029/90JA01975.

Weimer, D. R. (2004), Correction to "Predicting interplanetary magnetic field (IMF) propagation delay times using the minimum variance technique," *J. Geophys. Res.*, *109*, A12104, doi:10.1029/2004JA010691.

Weimer, D. R., D. M. Ober, N. C. Maynard, M. R. Collier, D. J. McComas, N. F. Ness, C. W. Smith, and J. Watermann (2003), Predicting interplanetary magnetic field (IMF) propagation delay times using the minimum variance technique, *J. Geophys. Res.*, *108*(A1), 1026, doi:10.1029/2002JA009405.